Mathematical Biosciences and Engineering

https://www.aimspress.com/journal/mbe

MBE, 23(4): 940–986.
DOI: 10.3934/mbe.2026037
Received: 30 November 2025
Revised: 06 February 2026
Accepted: 13 February 2026
Published: 03 March 2026

Review

Modeling neural dynamics with optical nonlinearity: From classical models to optogenetic approaches

Svetlana A. Gerasimova[1,2] **and Alexander N. Pisarchik**[3,*]

[1] Institute of Information Technologies, Mathematics and Mechanics, Lobachevsky University, Nizhny Novgorod, Russia

[2] Scientific and Educational Mathematical Center ´Mathematics of Future Technologies´, Lobachevsky University, Nizhny Novgorod, Russia

[3] Center for Biological Technology, Universidad Politécnica de Madrid, Pozuelo de Alarcón, Madrid, Spain

* **Correspondence:** Email: alexander.pisarchik@upm.es.

Abstract: Optogenetic experiments in vivo face fundamental limitations in real-time optical stimulation and biophotonic signal processing, constraining the efficiency and adaptability of neural circuit interrogation. This review establishes how photonic neuromorphic systems, operating at ultrafast speeds and with high energy efficiency, can overcome these barriers by forming a closed-loop optically driven interface with neural tissue. We present a comprehensive analysis of mathematical and computational models that describe neural dynamics in optical neuromorphic devices, bridging classical neuronal frameworks with optogenetic control paradigms. Emphasis is placed on how nonlinear dynamical modeling and data-driven approaches enable the design of photonic neurons and synapses capable of seamless integration with tapered fibers, fiber photometry, and computational optical control systems. Such integration allows real-time signal processing and adaptive feedback within optogenetic experiments, thereby enhancing precision and bidirectionality in living neural circuit interactions. By converging mathematical theory, photonic hardware, and neurobiology, this work provides a roadmap for next-generation neural interfaces that leverage optical neuromorphic computing to advance both intelligent neuroengineering and biomedical diagnostics.

Keywords: Optical neural networks; nonlinear photonics; neuromorphic computing; spiking photonic neurons; dynamical systems in neuroscience; bifurcation and nonlinear dynamics; integrated photonic circuits; temporal coding and signal processing; optogenetics and bio-inspired modeling

1. Introduction

The integration of optogenetics with mathematical modeling has established a new paradigm for analyzing and emulating neural computation. By enabling precise spatiotemporal control of neuronal activity in vivo through targeted photostimulation, optogenetics has revolutionized neuroscience [1–4]. This technique, which involves the genetic introduction of light-sensitive proteins, allows for the selective activation or inhibition of specific neurons and large ensembles [5–7]. It has become an indispensable tool for probing neural information processing and for developing novel therapeutic strategies for neurological disorders [8, 9]. Furthermore, when combined with simultaneous electrophysiological recording, targeted photostimulation has made optogenetics a cornerstone methodology for dissecting neural circuits, elucidating brain organization, and linking population dynamics to behavior [10–13]. The resulting high-precision, multimodal data now demands advanced mathematical frameworks capable of accurately modeling these controlled dynamics to bridge biological experiments with theoretical understanding.

Mathematical models that capture the effects of optical stimulation on neuronal dynamics serve a dual purpose: they advance our understanding of the underlying biophysics while providing a foundation for designing neuromorphic systems that exploit optical nonlinearities. Such modeling is particularly powerful for analyzing nonlinear phenomena like bifurcations, synchronization, and multistability in neural systems [14, 15]. Even reduced oscillator-based descriptions, such as the FitzHugh–Nagumo (FHN) [16, 17] and Hindmarsh–Rose (HR) [18] models, have proven effective in identifying key mechanisms of excitability and predicting neuronal responses to optical inputs. These models form a conceptual bridge between biological experiments and computational realizations, facilitating the design of photonic hardware that mimics neuronal dynamics.

Foundational works on neuromorphic modeling and neural circuit theory [19–21] established the principles of biologically grounded computation, from ion-channel kinetics to network-level behavior. Mathematical frameworks for neuronal dynamics [22] and multistability in biological systems [15] provided the theoretical basis for implementing realistic neural models in photonic and memristive hardware. Recent advances in computational neurology [23] further demonstrate the necessity of bridging biological realism with engineering constraints when designing neuromodulation devices. In this context, the control-oriented framework proposed by Martinez et al. [24, 25] formulates single-neuron and population-level models explicitly as nonlinear dynamical systems amenable to closed-loop control, highlighting observability, controllability, and model reduction as key prerequisites for feedback-based neuromodulation.

This control perspective is critical because traditional optogenetic systems often rely on predetermined, open-loop stimulation protocols, which limits their therapeutic efficacy and experimental precision. A paradigm shift toward closed-loop control requires real-time processing of neural activity to generate adaptive, activity-dependent stimulation. Here, neuromorphic photonic devices offer a compelling solution by enabling computation with sub-millisecond latency and minimal power consumption directly in the optical domain. Their integration with neural interface tools, such as tapered fibers for stimulation and fiber photometry for readout, can create a fully optical, adaptive control system [26, 27]. This computational optical control is essential for applications requiring continuous adaptation to brain state, such as seizure suppression or the restoration of sensorimotor function.

The limitations of conventional electronic architectures further motivate the development of optical neuromorphic platforms. In von Neumann computers, the separation between processing and memory units introduces latency and energy inefficiency at high operating speeds. Electronic circuits also struggle to match the ultrafast intrinsic response of optical components, a critical bottleneck for real-time biosignal processing. Physical scalability presents another challenge, as interconnect density restricts the construction of large-scale neural networks [28,29]. Optical systems, by contrast, naturally support high-bandwidth, low-latency, and energy-efficient parallel computation, making them ideally suited for implementing the neural models inspired by optogenetic principles. This convergence of optogenetics, mathematical theory, and photonic hardware paves the way for a new generation of intelligent, bidirectional interfaces with the brain.

This convergence is being driven by parallel advances in device technologies and their theoretical underpinnings. Foundational reviews have charted the landscape of neuromorphic photonics, from individual devices to full system architectures. Ferreira de Lima et al. [30] and Shastri et al. [31] surveyed the development of photonic neurons and synaptic devices, demonstrating operation at GHz speeds and energy efficiencies approaching 1 fJ/bit [32]. Fu et al. [33] provided a systematic analysis of optical neural networks, highlighting their inherent advantages in parallelism and throughput while identifying key challenges in thermal stability and the physical implementation of nonlinear activation functions. Complementary work by Song et al. [34] further emphasized scalability limitations and the pragmatic necessity for hybrid optoelectronic solutions. In parallel, researchers have explored memristive devices, where Yang et al. [35] and Huo et al. [36] detailed how ion-drift dynamics and phase transitions can be engineered to naturally exhibit spiking behavior and short-term memory, providing a distinct physical pathway to brain-inspired computation. Sun et al. [37] further reviewed architectures that leverage such devices for highly parallel, low-power processing. Meanwhile, at the bio-hybrid frontier, George et al. [38] demonstrated synaptic plasticity in systems that directly couple living neurons with electronic chips, blurring the line between biological and artificial computation. The neurophotonics community has concurrently developed a sophisticated toolkit for interrogation, with comprehensive surveys cataloging optogenetic actuators, including μLEDs, upconversion nanoparticles, and minimally invasive delivery methods, primarily as experimental techniques for dissecting neural circuits [39–41].

Despite this remarkable progress, a perceptible division persists in the literature. Work on photonic neural networks [30–34] is often oriented toward high-speed machine-learning computation, while research on memristive systems [35–37] focuses on analog in-memory computing and reservoir architectures. Both streams, however, frequently treat the mathematical description of device dynamics as a secondary concern rather than a primary design language. Consequently, three critical gaps remain at their intersection with neural engineering. First, existing reviews tend to prioritize device physics or computational performance, lacking a systematic treatment of the mathematical models, such as nonlinear rate equations and bifurcation analyses, that intrinsically connect photonic dynamics to the fundamental phenomena of neuronal excitability. Second, although optogenetics is extensively surveyed as a neuroscientific tool, the explicit integration of channelrhodopsin kinetics with the dynamical models of photonic neurons remains underexplored, creating a barrier to designing biophysically grounded, closed-loop interfaces. Third, prior work often addresses neuromorphic computing and biological neural systems in separate silos, without a unified framework for platforms that use photonic processing to directly control or emulate living neural circuits in real time.

This disconnect is becoming increasingly consequential. The 2025 neurotechnology roadmap explicitly calls for a transition from viewing optogenetics merely as an experimental methodology toward embracing it as a foundational principle for designing next-generation therapeutic neuroprostheses [42]. We argue that achieving this transition demands a deliberate multidisciplinary synthesis. It requires unifying the biophysics of light-neuron interactions, the engineering of photonic computing architectures [31,33], the nonlinear dynamics of memristive and optical systems [39], and the biological mechanisms of neural plasticity [38]. This review is positioned at this nexus, aiming to provide the missing integrative perspective by foregrounding mathematical modeling as the essential linchpin.

From an implementation perspective, photonic neuromorphic–optogenetic platforms can be viewed as a layered design flow progressing from elementary photonic building blocks toward system-level closed-loop operation. At the device level, this includes photonic neuron elements (e.g., microring resonators, passive microcavities, FP–SA lasers, VCSELs) and tunable weighting components (e.g., MZI meshes, resonator-based weights, or phase-change elements). These blocks are assembled into circuit-level primitives supporting weighted summation, nonlinear activation, and delay/feedback. At the subsystem level, wavelength-division multiplexing, fan-in/fan-out networks, and synchronization circuitry enables scalable neuromorphic processing. System-level integration combines the photonic processor with optical readout from neural tissue and programmable stimulation delivery. Finally, biological interfacing closes the loop by mapping measured neural states to stimulation waveforms, enabling adaptive optogenetic control.

Guided by this layered design flow, we introduce an experimental and technological roadmap (Figure 1) that translates these conceptual layers into a sequence of implementable stages. The roadmap systematically bridges the gap between foundational photonic components, scalable network implementations, and the feedback control required for adaptive bio-interfaces. This progression from isolated devices (a) to fully integrated systems (b) and closed-loop control architectures (c) demonstrates how photonic neuromorphic principles can be scaled to address the low-latency, high-bandwidth demands of real-time neural interfacing. Consequently, this integrative approach enables the development of targeted applications (d) that leverage photonic speed and parallelism for therapeutic and prosthetic interventions.

To this end, this review synthesizes rigorous mathematical models of computation with scalable photonic implementations to chart a systematic path toward intelligent, closed-loop neural interfaces. Our discussion is structured around three core, interdependent pillars:

- *Mathematical modeling of photonic neurons*: We analyze the dynamical systems—from passive microresonators to active laser oscillators—that replicate neuronal excitability, spiking, and refractory periods (Section 2).
- *Dynamics and plasticity in optical synapses*: We examine photonic and optoelectronic devices that implement synaptic weighting, filtering, and learning, discussing how their inherent dynamics often blur the classical neuron–synapse distinction (Section 3).
- *Architectures for network-level computation*: We review integrated photonic networks, highlighting how inter-component coupling, feedback, and system-level stability enable complex, brain-inspired computation (Section 4).

A control-theoretic perspective is woven throughout, as the envisioned optogenetic platforms are fundamentally feedback systems. Their behavior must therefore be interpreted through principles of nonlinear dynamics, stability, and sensitivity to parameter variations. This modeling foundation

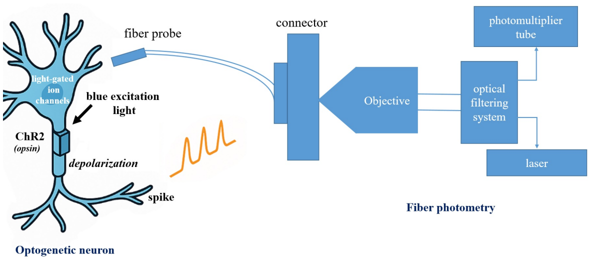

(a) Foundational components. Illustration of an optogenetic neuron with an integrated fiber photometry interface for optical readout.

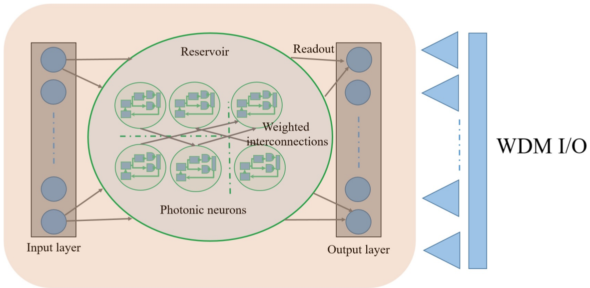

(b) Integrated neuromorphic processor. Schematic of a wavelength-division multiplexed (WDM) photonic reservoir computing chip for scalable neural network emulation.

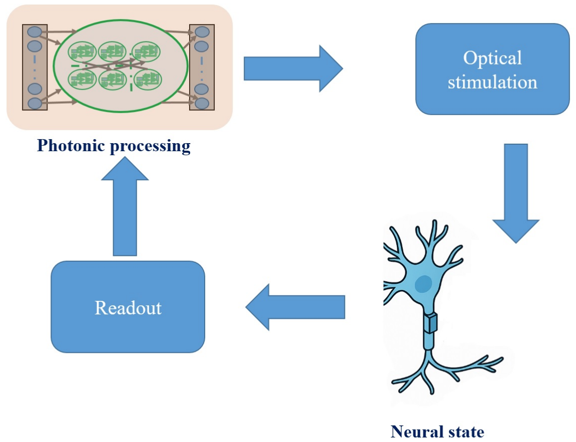

(c) Closed-loop control architecture. System diagram for adaptive neuromodulation, coupling photonic state processing with real-time optical stimulation.

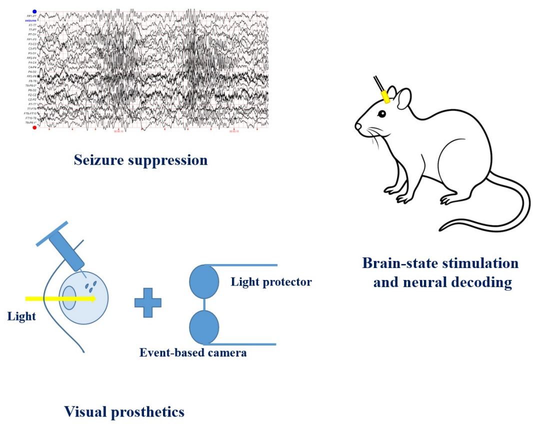

(d) Translational applications. Representative use cases enabled by the platform, including seizure suppression, brain-state decoding, and visual prosthetics.

Figure 1. An experimental roadmap for photonic neuromorphic–optogenetic systems. The progression from fundamental optoelectronic components (a) to integrated photonic networks (b) and finally to closed-loop bio-integrated control systems (c) charts a path toward real-world biomedical applications (d). This visual synthesis aligns with the layered design flow discussed in the text.

supports a dedicated discussion on optogenetic interfacing, where we integrate channelrhodopsin kinetics with photonic neuron models and frame the hybrid photonic–biological system as a controlled dynamical entity. The synthesis culminates in a conceptual blueprint for closed-loop neuromorphic–optogenetic platforms, directly informing the translational roadmap presented earlier. By foregrounding mathematical coherence, this review aims to bridge disparate device-centric literatures and establish a principled foundation for the next generation of neural prostheses and brain-inspired computing architectures.

2. Modeling photonic neurons: From microresonators to laser spikers

The implementation of neuronal excitability in photonic hardware relies on translating key dynamical features—threshold behavior, pulse generation, and a refractory period—into optical domain processes. Three primary device architectures exemplify this translation, each with distinct physical mechanisms and corresponding mathematical models:

- Passive microresonators: These cavities, lacking optical gain, leverage nonlinear Kerr effects or thermo-optic shifts to produce threshold-like activation and spike-shaped transmission.
- Fabry–Pérot lasers with saturable absorbers (FP-SA): This class of *active* neurons generates all-or-nothing optical spikes via a regenerative process of gain, absorption, and sudden energy release, closely mimicking biological action potentials.
- Microring resonators: Often used in coupled configurations, these versatile components provide essential signal processing functions such as temporal summation, filtering, and tunable delay, which are crucial for network integration.

Figure 2 illustrates representative configurations. Panels (a), (c), and (d) depict photonic neurons based on passive microresonators. These structures function as nonlinear filters or modulators, where spike-like responses emerge from resonance shifts induced by input power. Their compatibility with standard photonic integration platforms makes them attractive for scalable circuits. In contrast, the device in panel (b) represents the FP-SA laser, a fundamentally different, active architecture. Its spiking is an intrinsic oscillatory instability. When pump power exceeds a critical threshold, the coupled gain-absorber dynamics undergo a rapid, self-terminated transition, emitting a discrete optical pulse. This mechanism enables it to operate as a self-contained spike generator.

In the rest of this section, we survey the mathematical models that describe these systems, examining their characteristic dynamics, comparing their implementations, and assessing their roles within larger photonic networks.

2.1. Photonic passive microcavity neurons

Passive microcavity neurons emulate the core computational function of a biological neuron: the thresholded integration of incoming signals. These devices transduce a sustained or pulsed optical input into a discrete, spike-like optical output, effectively performing nonlinear filtering that mirrors neuronal excitability.

In a standard implementation, an optical input signal, typically in the 1310–1550 nm telecom range, is delivered via a waveguide to a passive, nonlinear microresonator. The resonator temporally integrates the input energy. Only when the accumulated intensity within the cavity surpasses a nonlinear threshold does the system undergo a rapid transition, emitting a sharp output pulse. This process is exemplified in architectures such as a vertical resonator formed by a rectangular protrusion: the input signal (often rectangular pulses with durations up to 1 ns, power levels of 1–10 mW, and repetition rates from kHz to 100 MHz) is filtered; upon exceeding a critical power, the resonator is excited and releases a distinct output spike, thereby converting a sub-threshold drive into a super-threshold, neuron-like response.

The dynamical behavior of a passive microcavity neuron is governed by a nonlinear differential

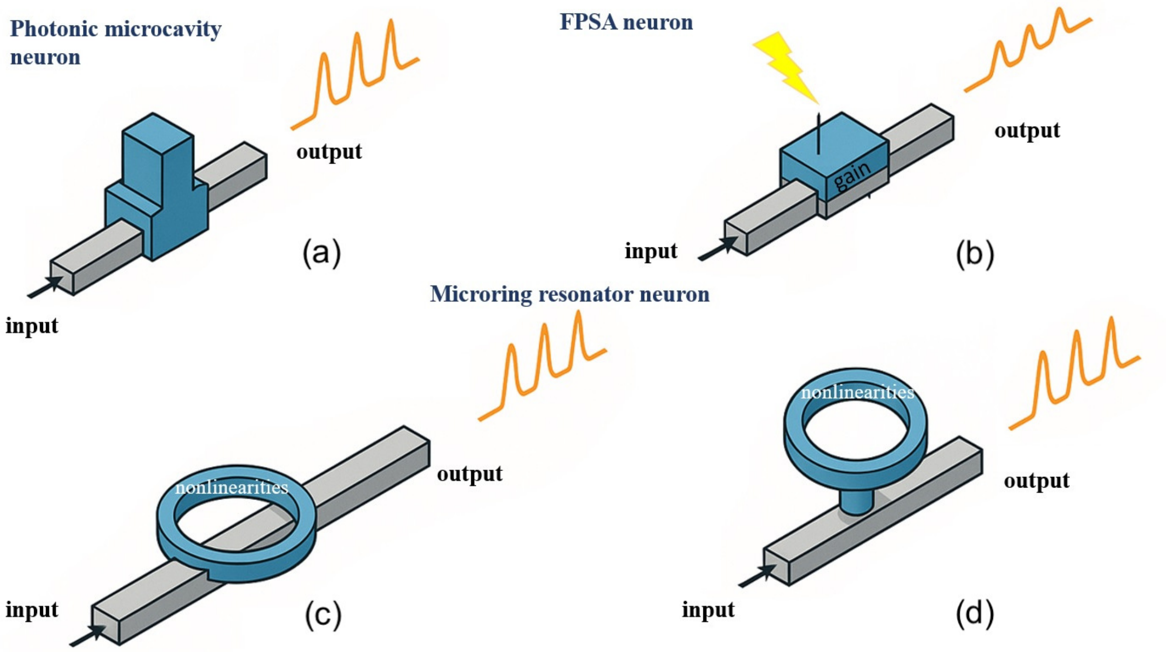

Figure 2. Representative architectures of photonic neurons. (a) A passive microresonator implementing threshold-like nonlinear filtering. (b) A Fabry–Pérot laser with a saturable absorber (FP-SA), functioning as an active spiking source. (c) A side-coupled and (d) an over-coupled microring resonator, enabling temporal summation and signal delay.

equation that serves as its computational core [43]:

$$\frac{dA}{dt} = (-\gamma + i\Delta\omega + ik|A|^2)A + \sqrt{\nu}\,S_{in}(t), \tag{2.1}$$

where $A(t)$ is the complex intracavity field amplitude, γ represents the total energy loss rate, $\Delta\omega$ denotes the frequency detuning between the input signal and the cavity resonance, k is the nonlinear Kerr coefficient, $S_{\text{in}}(t)$ is the input optical field, and $\nu \in [0, 1]$ quantifies the coupling efficiency between the waveguide and the resonator. This modeling framework is applicable to common integrated photonic platforms, including silicon (Si) and silicon nitride (SiN) [44].

In this formulation, $A(t)$ functions as the photonic analogue of a neuronal membrane potential, while its squared magnitude $|A(t)|^2$ corresponds to the measurable output intensity. The individual terms have clear physical and functional interpretations: $-\gamma A$ models cavity losses, $i\Delta\omega A$ introduces a detuning-induced phase shift, and $ik|A|^2A$ captures the intensity-dependent Kerr nonlinearity essential for threshold behavior. The driving term $\sqrt{\nu}S_{\text{in}}(t)$ injects the external optical field, with ν being determined by the resonator–waveguide interface geometry.

The system exhibits a sharp threshold response characteristic of neuronal excitability. For subthreshold input intensities, the intracavity field remains in a low-energy, quiescent state, as nonlinear effects are negligible. However, when $S_{\text{in}}(t)$ delivers sufficient energy within a short temporal window, the Kerr term $ik|A|^2A$ induces a dynamic shift of the cavity resonance. This initiates a positive feedback loop: the shifted resonance aligns more closely with the input frequency, enhancing energy coupling into the cavity, which in turn further amplifies the resonance shift. This regenerative process triggers a rapid, nonlinear buildup of the intracavity field, culminating in the abrupt emission of a spike-like output pulse. Following emission, cavity energy is depleted, and the system resets to equilibrium, thereby emulating the refractory period of a biological neuron.

Thus, the passive microcavity neuron acts as a nonlinear temporal integrator with a precise all-or-nothing activation mechanism. Its compact, all-photonic design and inherent compatibility with complementary metal-oxide-semiconductor (CMOS) fabrication processes establish it as a foundational building block for scalable photonic neuromorphic computing systems.

The theoretical framework of Eq. (2.1) has been progressively validated and refined through a series of landmark experimental and conceptual studies. This journey from foundational theory to system-level integration highlights the maturation of passive microcavities as versatile neuromorphic components. The vision for compact, energy-efficient photonic neurons was articulated early by Vahala [45], who described how microcavities with dimensions of $\sim 10\,\mu$m could generate ultrafast optical pulses (a few nanoseconds in width) with minimal energy. This conceptual framework established the promise of using strong light–matter interactions in confined geometries to build scalable, high-speed optical neural networks directly on silicon platforms.

A pivotal experimental milestone was achieved by Xiang et al. [46], who demonstrated the first fully passive photonic neuron using a side-coupled microring resonator. Their design exploited intrinsic nonlinearities—two-photon absorption, free-carrier generation, and thermal effects—to achieve thresholded excitation without active gain elements. This purely passive approach yielded nanosecond-scale spiking with sub-10 μW power consumption, marking a significant advance in simplicity, energy efficiency, and CMOS compatibility. Concurrently, Yang et al. [47] proposed a compact ($\sim 10\,\mu$m), ultrafast (spike width $\sim$4 ns) neuron design, further cementing the feasibility of integrating such elements into scalable silicon photonic circuits. The computational role of these devices was expanded beyond simple thresholding by Donati's monograph [48], which analyzed how nonlinear microring resonators can be harnessed for temporal data processing and spike generation, positioning them as versatile dynamical systems for analog computation and information encoding.

Subsequent research has explored more complex computational paradigms enabled by these devices. Castro et al. [49] systematically investigated how microresonator nonlinearities, cavity losses, and quality factor influence performance in reservoir computing, establishing a direct quantitative link between photonic device parameters and machine learning metrics such as state-space richness and computational capacity. The integration of silicon microring resonators into diverse architectures was further advanced by Biasi et al. [50], who demonstrated their utility across multiple computational paradigms, including feedforward networks, spiking models, and reservoir computing, highlighting their role as universal, reconfigurable building blocks for hybrid electronic–photonic platforms.

A critical consideration for the real-world deployment of these neurons, particularly within closed-loop systems, is their behavior in feedback configurations. In practice, passive microcavities are often embedded within optical or optoelectronic feedback loops, where small variations in detuning or cavity losses can significantly impact system stability and spike reproducibility. This sensitivity underscores the importance of the control-theoretic perspective highlighted earlier, linking device physics directly to requirements for robust, adaptive operation.

Collectively, these works trace the evolution of microring-based neurons from a compelling theoretical concept to a technologically mature and versatile platform for neuromorphic computing. From Vahala's initial vision and Xiang's passive implementation to their current role in complex computational architectures, this body of work demonstrates a clear pathway toward their integration into next-generation, closed-loop photonic processing systems.

2.2. Photonic neuron based on microring resonators

Building upon the foundational work discussed above, the microring resonator has emerged as a particularly mature and versatile platform for neuromorphic photonics, combining a compact footprint, CMOS compatibility, and rich nonlinear dynamics. In a typical operating regime, an optical signal, comprising a train of rectangular pulses with durations up to 1 ns, power of 40–60 μW, repetition rates from 1 to 10 MHz, and a wavelength near 1550 nm, is delivered to an input waveguide coupled to the resonator. The resonant circulation of light within the ring enables energy accumulation over multiple round trips. This process enhances the intracavity field until a nonlinear threshold is crossed, triggering the emission of a short optical spike at the output [51].

Two primary architectural configurations enable this neuron-like behavior. The first is the *side-coupled configuration*, where the microring is positioned adjacent to a straight waveguide. This geometry allows resonant coupling for spectral filtering, temporal summation, and signal delay. As a photonic neuron, it operates by integrating input energy until nonlinear phase shifts, driven by the accumulated intracavity power, precipitate a spike-like response.

The second approach utilizes *vertical (overlaid) coupling*, where the microring is fabricated directly above the bus waveguide. This 3D integration strategy enhances mode overlap and feedback strength, yielding a more compact and efficient device. Vertical coupling has been shown to facilitate stronger nonlinear interactions, self-oscillations, and robust threshold excitation, thereby expanding the repertoire of achievable neuronal dynamics.

Critically, both configurations inherently implement a biological *integrate-and-fire mechanism* paired with a *refractory period*, as detailed by Ye et al. [52]. The recirculation of light in the resonator provides temporal integration, while nonlinearities (e.g., the Kerr effect or free-carrier dispersion) induce dynamic resonance shifts. When the intracavity intensity reaches a threshold, this shift aligns the cavity resonance with the input wavelength, triggering a positive feedback loop that results in a sharp output spike. Following the spike, energy depletion and the subsequent relaxation of the cavity back to its equilibrium state mimic the neuronal refractory period. Under sustained input, this cycle produces repetitive spike trains that closely emulate the firing patterns of biological action potentials.

The experimental validation of the theoretical integrate-and-fire dynamics in microring resonators represents a cornerstone in the development of photonic neurons. A seminal demonstration by Shen et al. [53] implemented a silicon-based photonic neuron that utilized a microring resonator to produce a sharp, threshold-like transfer function, thereby closely emulating the input–output characteristics of biological neurons. The device successfully reproduced several fundamental neural behaviors:

- *Intensity threshold:* Activation occurred exclusively when the intracavity power accumulated beyond a critical level.
- *Spike-like output:* The system emitted sharp, well-defined optical pulses that captured the all-or-nothing character of biological action potentials.
- *Temporal integration:* The resonator effectively summed energy from consecutive sub-threshold input pulses, producing a spike only when the integrated energy exceeded the firing threshold.

These neuron-like properties arise directly from the physical interplay among resonant transmission, intracavity field buildup, and inherent material nonlinearities in silicon, such as the Kerr effect and free-carrier dispersion. The significance of this work is further underscored by the platform's full CMOS compatibility, positioning silicon microring resonators as highly promising candidates for large-scale neuromorphic integration, where compactness, scalability, and fabrication maturity are critical.

The dynamics of microring neurons are captured by an extension of the general nonlinear cavity model (Eq. (2.1)), which incorporates a feedback mechanism intrinsic to the ring geometry:

$$\frac{dA}{dt} = (-\gamma + i\Delta\omega + ik|A|^2)A + \sqrt{\nu}S_{in}(t) + \alpha A(t - \tau_f), \tag{2.2}$$

where α is the feedback strength, and τ_f is the roundtrip delay. This delayed feedback, arising from multiple roundtrips of light, enriches the system's dynamics by introducing recurrence and memory.

Unlike linear Fabry–Pérot microresonators, microring resonators enable multiple roundtrips of light, introducing temporal delays and cumulative phase effects that enrich their dynamic behavior. These features give rise to recurrence relations in the intracavity field, where each roundtrip's output depends on the evolving history of previous circulations. Such memory effects are fundamental to generating spikes, performing temporal summation, and achieving short-term dynamical storage, establishing microring resonators as versatile core elements for photonic spiking neural networks and reservoir computing architectures.

From a neurobiological perspective, the delayed feedback and resonance memory inherent to microring resonator neurons enable the emulation of complex neuronal behaviors, including temporal summation, self-excitation, spike adaptation, and refractory recovery, key hallmarks of biological spiking neurons. Unlike simpler passive resonators, microring-based neurons possess intrinsic memory due to optical feedback loops and non-instantaneous carrier dynamics, allowing them to replicate realistic spiking behavior with high fidelity. Consequently, microrings function not only as efficient nonlinear optical components but also as functional analogues of living neurons. Threshold photonic neurons based on microring resonators integrate ultrafast response times, low energy consumption, high integration density, and intrinsic optical nonlinearity. These properties make them promising candidates for neuromorphic photonic accelerators targeting real-time signal processing, temporal sequence learning, and pattern recognition, applications that leverage fast nonlinear dynamics and spike-based coding directly in hardware.

Recent experimental work has highlighted these capabilities. For instance, Yuan et al. [54] investigated passive microring resonators fabricated on a silicon-on-insulator (SOI) platform, with a resonance wavelength of 1552.77 nm, and revealed neuron-like self-oscillatory regimes. These oscillations arise from the interplay of two-photon absorption, free-carrier effects, and thermally induced resonance shifts, resulting in stable self-pulsations with a period of approximately 120 ns. Notably, the oscillation period is highly sensitive to resonance detuning ($\delta\lambda$), but only weakly dependent on input power. Furthermore, the authors demonstrated synchronization of multiple microrings via mutual coupling and cascaded delayed feedback. By using spike-timing mean squared error (MSE) as a synchronization metric, they achieved sub-nanosecond precision (MSE $< 10^{-6}$ for $\delta\lambda \in (0.002, 0.01)$ nm and feedback delay $\tau_f = 2$ ns), establishing the feasibility of networked microring neurons for reservoir computing and large-scale spiking networks in CMOS-compatible platforms.

Building on this foundation, Xiang et al. [55] extended microring-based neurons to computationally relevant tasks. They proposed and experimentally demonstrated photonic pulse-based convolution for feature extraction, integrated into a hybrid spiking convolutional neural network (SCNN). Their system achieved 94.1% classification accuracy on the Modified National Institute of Standards and Technology (MNIST) benchmark, demonstrating the potential of microring-based neurons for machine learning. To further highlight energy efficiency and scalability, they implemented a 5×4 photonic spiking neural network capable of pattern recognition tasks using ultralow-power spike-based processing.

In parallel, Tamura et al. [56] reported a CMOS-compatible photonic neuron architecture utilizing optical feedback in an electrically tunable microring modulator with a p–n junction. The system undergoes a subcritical Andronov–Hopf bifurcation, providing a versatile mechanism for switching between excitable and oscillatory regimes. The neuron's output is highly sensitive to both the amplitude and timing of input pulses, underscoring its suitability for time-domain information processing and temporal coding in neuromorphic circuits.

At the network level, Xu et al. [57] studied architectures for large-scale silicon photonic neural networks built from arrays of microring resonators. They focused on practical scalability challenges, such as wavelength variability, fabrication tolerances, and thermal cross-talk. The authors analyzed how deviations in resonance wavelengths (λ) propagate through the network and proposed compensation strategies to maintain performance in large integrated systems. This work provides critical insights into the feasibility of deploying microring-based neurons in densely integrated, chip-scale neuromorphic platforms.

Collectively, these studies highlight the versatility of microring resonators for neuromorphic photonics. Through their combination of nonlinear thresholding, temporal integration, self-oscillation, and synchronization, they emulate a wide range of neuronal behaviors while remaining fully compatible with silicon photonics technology. These advances pave the way toward scalable, ultrafast, and energy-efficient optical neural networks, bridging the gap between biologically inspired computation and practical photonic hardware.

2.3. Fabry–Pérot saturable absorber laser neuron

The Fabry–Pérot saturable absorber (FP-SA) laser represents a prominent class of *active* photonic neurons, integrating a Fabry–Pérot resonator with a saturable absorber (SA) to achieve biologically inspired spiking dynamics. In this configuration (Figure 2(c,d)), the device is excited with an optical input, i.e., typically rectangular pulses up to 1 ns in duration, 40–60 μW in power, at repetition rates of 1–10 MHz, and near 1550 nm, aligning with the dominant longitudinal mode of the cavity. Initially, at low intensities, the saturable absorber prevents transmission, effectively gating the optical signal. Once sufficient energy accumulates, the absorber saturates, leading to a rapid increase in transmission and the emission of a short, spike-like optical pulse, with a threshold energy on the order of 48 pJ. This mechanism inherently implements an "integrate-and-fire" response, complete with a refractory period, closely mirroring the activation and recovery cycle of a biological neuron.

The dynamics of an FP-SA neuron are typically described by a reduced two-variable rate-equation model:

$$\frac{dI}{dt} = [g_0 N - Q(I) - \gamma]\, I, \qquad \frac{dN}{dt} = P - \frac{N}{\tau_N} - g_0 N I, \tag{2.3}$$

where I is the intracavity intensity, N is the carrier density in the gain section, $Q(I)$ is the intensity-dependent saturable absorption, P is the pumping rate, γ accounts for cavity losses, g_0 is the differential gain coefficient, and τ_N is the carrier lifetime. This framework captures the core nonlinear processes: temporal integration, threshold activation, spike emission, and post-spike recovery. Unlike passive microresonator neurons, which rely on amplitude and phase dynamics (Eqs. (2.1) and (2.2)), FP-SA neurons are active devices where spiking is driven primarily by energy accumulation in the gain medium and its abrupt release upon absorber saturation.

As excitable oscillators, FP-SA neurons exhibit dynamics that are strongly governed by feedback topology and parameter sensitivity. Key control parameters, such as gain coefficient g_0, absorber recovery time, and external modulation depth, directly influence the lasing threshold, spike timing, and overall stability. This sensitivity underscores their suitability for closed-loop architectures, where precise tuning enables adaptive, real-time neuromorphic processing.

FP-SA lasers have thus emerged as a central platform for neuromorphic photonics. Xiang et al. [58] demonstrated an integrated FP-SA laser neuron chip capable of temporal integration, threshold-triggered spiking, and refractory recovery, and further proposed temporal spike multiplexing to address hardware scalability. Zheng et al. [59] experimentally validated coherent photonic neural computing using FP-SA lasers, confirming their feasibility for neuron-like signal processing. Fu et al. [60] reviewed the broader role of semiconductor lasers with saturable absorbers in neuromorphic computing, identifying FP-SA lasers as a promising active element for implementing neural dynamics. Recent contributions by Shi et al. [61] and Song et al. [62] further highlight their potential for constructing high-speed, low-power photonic spiking neural networks.

A fundamental distinction between active FP-SA neurons and passive microcavity or microring neurons lies in the presence of optical gain. Active neurons incorporate a pumped gain medium (electrically or optically pumped) enabling energy accumulation and autonomous spike generation. In contrast, passive neurons lack optical gain and instead rely on intensity-dependent losses, carrier-induced index changes, or thermo-optic effects to produce threshold dynamics. While passive architectures (e.g., silicon microrings) benefit from CMOS compatibility and scalability, active FP-SA neurons offer richer dynamical regimes, such as excitable responses, relaxation oscillations, and self-pulsations, due to the interplay between gain and loss.

Despite these structural differences, all three major photonic neuron architectures (passive microresonators, microring resonators, and active FP-SA lasers) share core functional attributes: threshold activation, spike emission, and refractory behavior, supporting fully optical input–output processing without electronic conversion. These common features enable spike-based coding, temporal integration, and logic operations in neuromorphic circuits. In summary, passive devices offer compactness, scalability, and energy efficiency, while active FP-SA lasers provide enhanced dynamical richness and controllability. Together, they establish a versatile hardware foundation for large-scale, ultrafast photonic spiking neural networks with applications in low-power neuromorphic computing and adaptive neural interfaces.

Nonlinear optical effects, and, in particular, Kerr nonlinearity, play a central role in enabling thresholding, gain, and neuron-like activation in purely photonic systems.

2.4. *Kerr effect–based signal amplification*

Third-order Kerr nonlinearity $\chi^{(3)}$ plays a central role in implementing neuron-like functionalities in photonic systems. The Kerr intensity-dependent refractive index, $n = n_0 + n_2|E|^2$, leads to a cubic nonlinearity with respect to the field amplitude, giving rise to optical bistability—a phenomenon in which a resonator exhibits two stable transmission states at the same input power [63, 64]. This results in an S-shaped transfer characteristic analogous to the sigmoidal activation function in biological neurons, which is critical for realizing threshold elements and nonlinear information processing in photonic neural networks. Furthermore, self-phase modulation induced by the Kerr effect enables intensity-dependent phase shift, thereby extending the functional richness of neural network architectures [65].

Signal amplification can be achieved by exploiting Kerr nonlinearity under strong optical pumping. The dynamics of a Kerr optical resonator are governed by the same cubic nonlinear cavity equation as introduced in Eq. (2.1), with the Kerr term providing the physical origin of optical bistability and neuron-like threshold behavior. To analyze the small-signal gain, the intracavity field is decomposed into a stationary strong pump component a_0 and a small signal fluctuation: $a = a_0 + a_s$, where $|a_s| \ll |a_0|$. After substituting into the original equation and linearizing around the steady state, we obtain the effective parametric gain equation for the signal component:

$$\frac{da_s}{dt} = (i\Delta_{eff} - \kappa)a_s + iGa_s^{\dagger}e^{i\phi}, \tag{2.4}$$

where a_s is the signal photon annihilation operator, $a_s^{\dagger}$ is the signal photon creation operator, $\Delta_{eff} = \Delta - 2\chi^{(3)}|a_0|^2$ is the effective Kerr detuning of the resonator, Δ is the bare cavity–pump detuning, ϕ is the interaction phase, and $G = \chi^{(3)}|a_0|^2$ is the pump-induced Kerr coupling coefficient.

This $\chi^{(3)}$-mediated interaction enables all-optical amplification via four-wave mixing in high-Q photonic resonators or nonlinear waveguides [66, 67]. The gain coefficient can be estimated as $G = \gamma P_p$, where P_p is the circulating pump power, and γ is the nonlinear Kerr coefficient of the material. The amplification regime remains compatible with quantum-limited operation down to the single-photon level, provided that the standard noise constraints of Kerr parametric amplification are satisfied [68, 69].

The combination of bistability, amplification, and self-phase modulation within a single Kerr platform opens pathways toward fully integrated optical neural networks with multifunctional nonlinear elements.

2.5. Comparative discussion: Passive versus active photonic neuron architectures

A comparative analysis of photonic neuron architectures reveals fundamental trade-offs between passive and active designs, governed by their underlying physical mechanisms and their implications for system-level performance. The choice between these approaches hinges on the specific requirements of the target application, balancing dynamic richness against practical constraints such as power, scalability, and fabrication complexity.

Passive neurons, implemented in silica, silicon nitride microcavities, or silicon microring resonators, derive their functionality from intrinsic material nonlinearities, such as the Kerr effect, free-carrier dispersion, or thermo-optic shifts. Their primary advantages lie in exceptional compactness, ultralow static power consumption, and seamless compatibility with large-scale CMOS photonic integration [51–53]. These devices successfully emulate core neuronal features, including temporal integration, threshold activation, and all-or-nothing spiking. However, their dynamics are inherently driven by external optical excitation; they lack an internal gain medium and therefore cannot autonomously generate sustained spiking or oscillatory activity without additional feedback or amplification circuits. This makes them ideal for scalable, energy-efficient networks where individual nodes are externally driven.

Active neurons, most notably Fabry–Pérot lasers with integrated saturable absorbers (FP-SA), incorporate optical gain, typically via electrical or optical pumping. This gain medium enables energy accumulation and regenerative feedback, supporting a richer suite of nonlinear behaviors—including excitable spiking, relaxation oscillations, and self-sustained pulsations [58–60]. These dynamics more closely mimic the energetic and temporal characteristics of biological neurons. The trade-off, however, is increased architectural complexity, higher power demands to maintain population inversion, and greater challenges in dense integration compared to their passive counterparts.

In summary, passive architectures offer a path toward ultra-efficient, highly scalable neuromorphic circuits, while active architectures provide enhanced dynamical control and autonomous signal generation. The selection of one approach over the other, or their hybrid integration, depends on the application's priorities: whether maximizing component density and energy efficiency or leveraging complex, self-sustained dynamics for advanced computational tasks. Together, these complementary paradigms expand the design space for photonic neuromorphic systems, enabling tailored solutions across computing, sensing, and bidirectional neural interfacing.

From an application standpoint, the architectural choice between passive and active neurons is dictated by system-level priorities. Passive photonic neurons are ideally suited for massively parallel, low-power neuromorphic accelerators where energy efficiency and scalability are critical, such as in reservoir computing and large-scale signal pre-processing pipelines [49, 50]. In contrast, active FP-SA neurons excel in applications demanding richer, self-sustained dynamics, such as autonomous oscillatory regimes, flexible excitability control, or complex temporal coding, making them strong candidates for feature extraction, time-series processing, and hybrid optoelectronic systems [61, 62]. A promising direction lies in hybrid integration, where passive microring neurons and active FP-SA elements are combined on a shared silicon photonics platform. This approach could optimally balance the scalability and efficiency of passive devices with the dynamical versatility of active components.

A systematic comparison of these architectures is presented in Table 1, which evaluates ten critical parameters across three representative implementations. These parameters include material platform, spiking behavior, oscillation frequency, activation threshold, CMOS compatibility, control mechanism, synchronization strategy, scalability, power consumption, and feedback implementation. The analysis reveals clear trade-offs: passive microcavities (Si/SiN-based) offer superior CMOS compatibility and minimal static power but require external optical drive; FP-SA lasers enable autonomous spiking through internal gain but face material and power overhead challenges; microring resonators occupy an intermediate space, combining nonlinear thresholding with inherent delayed feedback for synchronization.

The substantial progress in photonic computing reflected in this comparison suggests that fully functional photonic neuromorphic processors are becoming increasingly viable. These advances are stimulating interdisciplinary innovation and positioning photonic platforms as competitive candidates for next-generation, high-speed, energy-efficient computing. However, a fundamental conceptual divergence from biology persists. In current photonic implementations, the classical biological distinction between neuronal and synaptic elements is inherently blurred. A single nonlinear microresonator often performs dual roles: it acts as a spiking neuron (integrating and firing) and as a signal-transmitting synapse (applying weighting and temporal filtering). This functional merging means that neuron-like computation is achieved within unified physical devices, and the separation between neuronal and synaptic functions becomes primarily a network-level architectural consideration rather than a dis-

Table 1. Comparative characteristics of photonic neuron architectures, including material platform, activation threshold, power consumption, CMOS compatibility, and integration scalability.

Feature	Photonic passive microcavity neuron	Fabry–Pérot saturable absorber laser neuron	Microring resonator neuron
Material	Si, SiN	III-V (InGaAsP, GaAs)	Si, SiN
Spike-like behavior	Self pulse	LIF-spikes	Self pulse, spikes
Oscillatory frequency	~5–10 MHz	~500 MHz	~5–10 MHz
Threshold	~mW	Voltage/current (mA)	Depends on detune and input
CMOS-compatibility	✓	×	✓
Control	λ, temperature	Current, voltage, optical injection	λ, temperature, delay
Synchronization	Through detune	Through optical injection and SA	Through feedback and detune
Scalability	High	Limited by current and heat	Medium–high
Energy consumption	Low	High	Low
Feedback	External optics	Through cavity and SA	Feedback via delay loop

crete hardware distinction. This represents a paradigm shift from biomimetic design toward function-optimized photonic processing, with significant implications for learning algorithms, network scalability, and biological interpretability.

2.6. Optogenetics and photonic neurons

A powerful technological convergence is emerging between the fields of optogenetics and neuromorphic photonics, both fundamentally reliant on light as a means of information transfer and control (Figure 3). While optogenetics employs light to probe and modulate living neural circuits via genetically encoded actuators like channelrhodopsin-2 (ChR2) and halorhodopsin [70–72], neuromorphic photonics implements neural network models directly in hardware using light. The synergy lies in developing hybrid photonic–biological interfaces capable of bidirectional, closed-loop communication: photonic systems can deliver precise optogenetic stimulation while simultaneously processing optical readouts (e.g., fluorescence, scattering) from the neural tissue.

This integrated approach enables the physical emulation of key biophotonic processes, such as intracellular signaling, fluorescence dynamics, and light-triggered ion flux, to create platforms that can (1) systematically analyze the efficacy of optogenetic protocols on neuronal ensembles, (2) identify optical stimulation patterns that induce stable functional changes (e.g., neural plasticity), and (3) train neural network models under biologically realistic, variable conditions. The result is a tight methodological alignment where light serves as both a precise probe and a programmable control signal, bridging photonic engineering and experimental neuroscience.

A critical distinction from biological systems, however, lies in the functional architecture of the photonic hardware itself. In many integrated implementations, the classical biological separation between neuronal and synaptic elements is not preserved. As illustrated in Figure 3, a single photonic device, such as a microring resonator, an FP-SA laser, or a phase-change material (PCM) cell, can simultaneously exhibit neuron-like functionalities (nonlinear activation, thresholding, excitability) and synapse-like functionalities (weighting, temporal filtering, analog memory). This functional overlap is not a limitation but a direct consequence of photonic design, where nonlinearity, signal routing, and memory are naturally co-localized within the same physical element. While this reduces one-to-one biological interpretability, it represents a deliberate hardware optimization that enhances compactness, bandwidth, and scalability. Consequently, learning in such systems does not rely on a strict modular separation between neurons and synapses but instead on the reconfigurability and integrated memory of each device, enabling highly parallel and hardware-efficient implementations. This architectural paradigm is particularly advantageous for constructing closed-loop optogenetic interfaces, where processing efficiency and minimal latency are paramount.

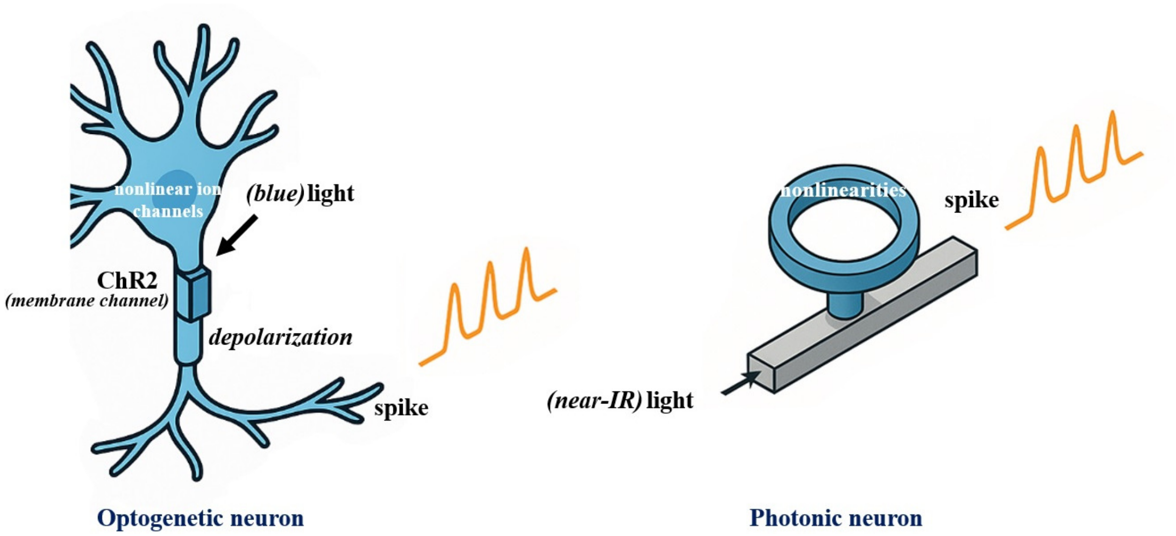

(a) (b)

Figure 3. Comparison of spike-generation mechanisms in optogenetic and photonic neurons. (a) In an optogenetically modified neuron, light activates channelrhodopsin-2 (ChR2) ion channels, inducing membrane depolarization and triggering a biological action potential. (b) In a photonic neuron, an input optical pulse drives nonlinear dynamics (e.g., Kerr effect, carrier-induced shifting) within a microresonator, leading to the emission of an optical spike. In both systems, optical stimulation initiates excitable threshold dynamics that culminate in an all-or-nothing output spike.

This convergence establishes a foundation for adaptive, bidirectional neural interfaces that leverage the speed and parallelism of light for both observation and intervention, paving the way for next-generation neuroprosthetics and brain–machine communication systems.

Notably, experimental studies have demonstrated that near-infrared light exposure can modulate hippocampal neuronal activity through non-genetic means [73]. These effects are attributed primarily to physical mechanisms (thermal, mechanical, and photochemical interactions) rather than genetically encoded photosensitivity. Crucially, the resulting neural responses exhibit cumulative and irregular dynamics, contrasting sharply with the precise, threshold-activated spiking enabled by optogenetic tools. Research in this domain [74–77] is therefore critical for developing non-invasive neural modulation strategies and neurohybrid systems, where precise control is essential but genetic modification must be avoided.

A profound physical analogy underlies both photonic neural networks and optogenetics: in each case, light drives nonlinear processes within a medium, altering its state as a function of intensity, duration, and stimulation history. This conceptual proximity enables optical neuromorphic systems to serve as high-speed physical emulators for modeling, simulating, and optimizing optogenetic experiments.

The use of advanced photonics in optogenetics has a well-established history. For example, two-photon absorption allows activation of retinal chromophores using infrared light (920–1060 nm), penetrating 500–800 μm of tissue with a subcellular excitation volume of $\approx$2–3 μm^3 [78, 79]. Three-photon excitation extends access to subcortical layers (> 1 mm) but requires peak intensities exceeding 100 GW$\cdot$cm^{-2}. A fundamental constraint is photocurrent saturation, where increasing optical power beyond a certain point yields no greater neural response while phototoxicity continues to rise.

Photonic hardware can directly emulate these biophysical dynamics. Optical resonators with embedded nonlinear materials (e.g., Kerr media) can be tuned—via quality factor and nonlinear coefficients—to reproduce characteristic opsin response curves, including temporal constants and saturation profiles. Similarly, optical memristors can mimic multi-state opsin kinetics (e.g., the four-state model of ChR2(H134R) [80]) through material phase changes. Crucially, photonic networks process spatial light patterns natively, enabling real-time emulation of how opsin-expressing neuronal populations respond to the profile of a laser beam. This capability is vital for planning large-scale experiments, such as patterned stimulation of the visual cortex.

Such systems can thus function as ultrafast physical emulators to identify optimal stimulation parameters (pulse shape, frequency, spatial distribution). Their intrinsic picosecond-to-nanosecond response times far exceed software simulation speeds, allowing for rapid exploration of protocol space using optimal control principles [81]. This addresses a growing need in the field, where software platforms like PyRhO, which evolved from a descriptive kinetic model [80] into a comprehensive simulation tool [82], are ultimately constrained by digital hardware performance.

A hybrid framework integrating photonic neuromorphic accelerators with software like PyRhO could deliver transformative advantages:

- Acceleration: 100–1000 times faster simulation of large networks (> 10^5 neurons) via optical parallelism.
- Efficiency: Ultra low energy consumption (fJ per operation vs. pJ in digital hardware).
- Integration: Seamless use of the same optical source and pathway for both simulation and subsequent biological experiment.

This approach has direct clinical relevance. Projects like PIONEER (GS030), which uses AAV–ChrimsonR to restore vision in retinitis pigmentosa, require patient-specific tuning of stimulation parameters. Photonic neuromorphic systems could act as personalized physical emulators, predicting optimal protocols based on individual opsin expression and retinal topology in real time, using the very optical hardware intended for therapy.

A promising pathway for non-invasive neural interfacing leverages the ability of near-infrared (NIR) light to modulate hippocampal activity [73]. This effect stems from physical mechanisms like thermal and photochemical interactions, not from genetic encoding. The resulting dynamics are inherently cumulative and irregular—a fundamental divergence from the crisp, threshold-driven responses of optogenetics. This very distinction makes NIR stimulation a critical area of study [74–77] for developing next-generation neurohybrid systems and therapeutic strategies where genetic modification is prohibited, yet high-fidelity control is paramount.

In conclusion, integrating photonic neuromorphic systems into the optogenetic workflow is both technically feasible and conceptually powerful. The structural analogy between optical nonlinearities in hardware and photodynamics in biology provides a natural correspondence, paving the way for specialized optical accelerators that bridge neurobiological computation and therapeutic intervention.

3. Optical synapses: Photonic implementation and plasticity models

The development of optical synapses is a critical step toward building ultrafast, energy-efficient neuromorphic processors. These components replicate the core function of biological synapses, transmitting and adaptively weighting signals between computational units, but do so using light. This enables high bandwidth, low latency, and low crosstalk, which are essential for scalable neural networks.

Foundational optoelectronic implementations established the basic principles of optical synaptic coupling. An early, influential model used an infrared LED and photodiode pair to couple two FHN electronic oscillators [83]. In this system, the state of one oscillator modulated the light intensity driving its partner, creating an all-optical feedback loop. By tuning coupling parameters, fundamental synchronization regimes, including complete and phase-locked synchronization, were demonstrated. This work proved that light could effectively transmit timing information and orchestrate coordinated dynamics between artificial neurons, establishing a minimal blueprint for an optical synapse.

The transition to integrated photonic platforms marked a shift toward higher speed, greater complexity, and biophysical realism. A significant advance utilized erbium-doped fiber lasers (EDFLs) as optical drivers [84–86]. Here, an FHN oscillator modulating an EDFL's pump could induce rich nonlinear dynamics, including chaos and multistability, in a receiving laser neuron. This paradigm was later extended to the three-variable Hindmarsh–Rose model [87], which reproduces biologically realistic activity patterns like bursting and chaotic spiking. These studies demonstrated that optical synaptic links could mediate sophisticated, patterned interactions far beyond simple pulse forwarding.

The field is now advancing toward all-optical networks with embedded plasticity, where synaptic functionality is fully integrated into photonic circuits. This shift moves beyond simple point-to-point optical links to engineer essential network-level properties: signal routing, fan-in and fan-out, and, most critically, synaptic plasticity. In biological systems, activity-dependent adjustment of connection strength forms the foundation of learning and memory. In photonics, this is realized through devices whose transmission or phase shift can be dynamically modified by optical signals, enabling the direct hardware implementation of learning rules such as spike-timing-dependent plasticity (STDP).

A fundamental architectural departure from biology is the frequent functional overlap between neurons and synapses in integrated photonic platforms. In many implementations, a single element, such as a nonlinear resonator or interferometer, can simultaneously perform thresholding (a neuron-like function) and signal weighting or temporal filtering (a synapse-like function). This co-localization is a deliberate hardware optimization that enhances compactness, speed, and energy efficiency, though it necessitates a rethinking of network design and learning algorithms away from strict biological analogy. Consequently, optical synapses are no longer conceived as isolated links but as integral components within large-scale, distributed photonic architectures.

In the following subsections, we examine the mathematical models of plasticity governing these systems and detail the state-of-the-art hardware implementations that underpin next-generation neuromorphic computing.

3.1. Phase-change material synapses and photomemristors

Phase-change materials (PCMs) offer a powerful platform for implementing artificial optical synapses, where the synaptic weight is encoded in the material's structural phase. This subsection outlines the operational principle, theoretical description, and device realizations of PCM-based synapses, and introduces the closely related concept of the photomemristor.

The core functionality relies on the reversible, laser-induced phase transition of a PCM thin film (e.g., $Ge_2Sb_2Te_5$ or GST225) between an amorphous state and a crystalline state. These two phases exhibit distinct optical properties, such as absorption and refractive index. The synaptic weight is defined by controlling this phase: a "write" laser pulse (typical parameters: $\lambda \approx 532$ nm, duration $\approx 10 - 30$ ns, intensity $\approx 1 - 4$ MW/cm^2) selectively heats the material to induce a phase change. Subsequently, a separate "read" probe signal (often at telecom wavelengths like $\lambda \approx 1550$ nm) is modulated in intensity or phase by the film, thereby reading the stored synaptic weight that governs signal transmission between photonic neurons [88–90].

The dynamical response of a PCM synapse to optical pulses is governed by a coupled thermo-optical model [91]. This model integrates three key physical processes:

1. Heat diffusion: Describes the temperature evolution $T(t, \mathbf{r})$ due to absorption of the control laser pulse [92].
2. Phase transition kinetics: Models the evolution of the crystalline fraction $C(t, \mathbf{r})$ ($C = 0$: amorphous, $C = 1$: crystalline) [93].
3. Optical readout: Relates the material's phase state to the transmission of the probe beam [94].

These processes are captured by the following system of equations, which together emulate synaptic plasticity:

$$\rho c_p \frac{\partial T}{\partial t} = \nabla \cdot (k(C)\nabla T) + Q_{abs}(t), \tag{3.1}$$

$$\frac{\partial C}{\partial t} = k_{cryst}(T) \cdot C \cdot (1 - C), \tag{3.2}$$

$$I_{out} = I_{in} \cdot \exp\left(-k_{ext}(C) \cdot d\right). \tag{3.3}$$

Here, Eq. (3.1) is the heat diffusion equation, where ρ is density, c_p is heat capacity, $k(C)$ is thermal conductivity, and $Q_{abs}(t)$ is the absorbed laser power density. It calculates the localized heating profile critical for precise phase transitions. Eq. (3.2) governs the crystallization kinetics using a Johnson-Mehl-Avrami-type formalism. The temperature-dependent rate $k_{cryst}(T)$ and the term $C(1-C)$ ensure that the phase change slows as it nears completion. The evolution of C is the direct physical analogue of the synaptic weight update. Finally, Eq. (3.3) describes the optical readout via the Beer-Lambert law. The output probe intensity I_{out} is attenuated based on the extinction coefficient $k_{ext}(C)$, which depends on the phase, and the film thickness d.

This theoretical framework has been experimentally validated in various photonic platforms using GST225. The implementations share the principle of all-optical control but differ in topology, leading to varied performance metrics:

- Waveguide-integrated films: Depositing thin GST225 films on polymer or Si_3N_4 waveguides [95, 96] enables direct modulation of guided light. These devices show transmission changes up to $\sim 40\%$ (≈ 7 dB) with pulse energies of ~ 486 pJ, and have demonstrated multi-level storage (e.g., 16 states) and optical spike-timing-dependent plasticity (STDP) learning rules.
- Enhanced photonic structures: Integration with resonant structures like photonic crystals [97] or directional couplers [98] enhances light-matter interaction, allowing for more efficient control over coupling ratios and lower energy switching.
- Ultracompact plasmonic and nanogap devices: Employing plasmonic effects or nanoscale gaps [99, 100] achieves extreme miniaturization (footprint < 1 μm^2), high optical contrast ($> 74\%$), and low energy consumption ($\approx 8-42$ pJ per event). These features are pivotal for high-density, scalable neuromorphic photonic circuits.

A closely related and advanced paradigm is the *photomemristor* [101]. While the term "PCM synapse" often implies a separated "write" and "read" process, a photomemristor is defined by a direct, nonlinear relationship between the history of input optical stimuli and the resulting optical response, exhibiting persistent memory and hysteresis [102–104]. The term "photomemristor" has gained significant traction since circa 2018, formalizing the extension of the memristive concept, where device state depends on the history of stimuli, into the optical domain.

For PCM-based devices, the theoretical model (Eqs. (3.1)–(3.3)) remains applicable. The conceptual shift is in the operational paradigm: in a photomemristor, the same optical port or beam can be used for both writing the state (via pulse intensity/duration) and reading it (via transmitted/reflected power), without intermediary electrical conversion [105, 106]. The continuously variable crystalline fraction $C(t)$ thus directly translates into a continuously variable optical transmission, making photomemristors ideal, compact building blocks for representing synaptic weights in all-optical neural networks.

The integration of PCM synapses and photomemristors into larger, functional photonic neural network architectures is a vibrant research frontier. Current efforts focus on achieving scalable interconnect schemes, demonstrating on-chip learning algorithms, and co-designing devices with photonic neurons to realize fully photonic, efficient, and high-speed neuromorphic computing systems.

3.2. Implementation of photomemristive synapses

Photomemristors represent an advanced class of devices in neuromorphic photonics, defined by their *all-optical* memory and programmability. This subsection details their operational paradigm, key application in neuromorphic vision, performance benchmarks, and integration into reconfigurable photonic systems.

The photomemristor conceptually merges the non-volatile memory function of an electronic memristor with purely optical control and readout. Its defining characteristic is a direct, history-dependent relationship between optical input (stimulus) and optical output (response), without intermediate electrical signals. As illustrated in Figure 4, this contrasts with hybrid optoelectronic synapses and even some PCM devices that may separate optical "write" and electrical "read'"processes. In a photomemristor, the same optical pulse can both alter and probe the device state, leading to inherent memory and hysteresis in the optical domain [101, 102]. This seamless fusion of memory and photonic modulation makes them ideal for direct, in-sensor processing of optical data.

A primary and promising application of photomemristors is in neuromorphic vision systems, where they enable *in-sensor computing* by colocating sensing, memory, and processing. Device arrays function as both pixellated sensors and programmable synaptic weight matrices. For example, CMOS-compatible photomemristor arrays (scalable to 10×10 pixels) have demonstrated long-term image retention without power and achieved up to 86.7% accuracy in face recognition tasks [107, 108]. These systems emulate key biological learning rules, such as short-term plasticity (STP), long-term potentiation (LTP), and spike-timing-dependent plasticity (STDP), across a broad optical bandwidth (ultraviolet to near-infrared). Integration with plasmonic nanostructures (e.g., via localized surface plasmon resonance, LSPR) further enhances light-matter interaction, improving both optical efficiency and pattern learning accuracy [108].

The performance of photomemristive synapses is benchmarked by three critical metrics essential for scalable neuromorphic hardware:

- Speed and temporal resolution: Implementations using phase-change materials (e.g., GST) in silicon waveguides have been switched with picosecond optical pulses ($\lambda \approx 1570$ nm), achieving state changes with a temporal resolution exceeding 1 ns [109]. This surpasses the speed limits of most electronic memristors.
- Energy efficiency: The energy per switching event for these integrated devices can be below 100 pJ, with advanced plasmonic and nanoscale designs reaching the 10–100 pJ range [109, 110].
- Analog behavior and retention: Photomemristors exhibit high-fidelity multi-level analog storage, with demonstrations of up to 32 distinct, non-volatile states, crucial for emulating the analog nature of biological synaptic weights.

This combination of high speed, low energy, and analog programmability provides a seamless interface with photonic integrated circuits and fiber-optic networks.

Beyond standalone synapses, photomemristors are engineered as the active element in reconfigurable nanophotonic circuits. By integrating PCMs (GST, Sb_2S_3) into the core of photonic components, researchers have demonstrated light-programmable control over fundamental optical properties. For instance:

- Programmable waveguides: The phase and amplitude of guided light can be dynamically tuned by locally switching the PCM state, enabling reconfigurable interferometers and filters.
- Tunable metasurfaces: Integrating PCMs into metasurface unit cells allows for post-fabrication control over beam steering, spectral response, and polarization manipulation with sub-wavelength precision [110].

These systems achieve reconfiguration with ultralow energy (10–100 pJ per switch) and are fully compatible with standard silicon photonics platforms, paving the way for dynamically programmable photonic neural networks on a chip.

While traditional memristors rely on electronic signals and ionic migration to modulate resistance, photomemristors utilize optical excitation to induce persistent changes in their optical properties. This fundamental distinction in operating principle is illustrated in Figure 4.

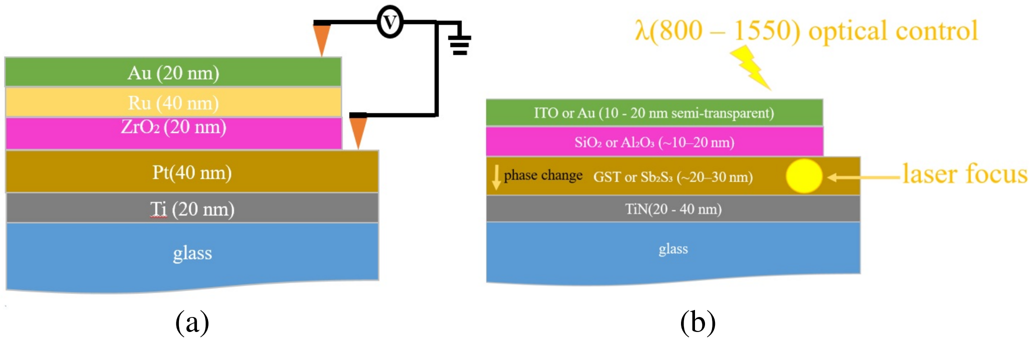

Figure 4. Contrasting switching modalities in memristive devices. (a) Electro-ionic switching in a ZrO_2 memristor, where filament formation/rupture via cation migration under a bias alters resistance. (b) All-optical switching in a photomemristor, where a phase transition in a chalcogenide material (e.g., GST, Sb_2S_3) is directly induced by photonic energy ($\lambda = 800 - 1550$ nm). The layered material schematics underscore the different physical domains exploited for non-volatile state control.

As shown in Figure 4, the switching mechanisms of electrical and photomemristors are fundamentally different. In the electrical memristor (a), resistance is modulated by the electric-field-induced migration of oxygen vacancies (O^{2-}). In contrast, the photomemristor (b) is switched optically, with a focused laser pulse inducing a localized phase change. Both device architectures incorporate functional upper and lower layers essential for thermal management and optical interfacing, highlighting a design commonality despite their distinct stimuli.

The study of these complementary memristive phenomena is pivotal for neuromorphic engineering. Building on foundational work in thin-film devices and networks [111–117], Table 2 synthesizes a comparative analysis of their operating principles and key performance characteristics.

The fundamental difference in stimuli—electrical versus optical—naturally leads to distinct roles in neuromorphic architectures. In such systems, memristors serve as artificial synapses, while the source of the control signal (electrical or optical) functions as the neuron [118]. Consequently, in a conventional memristor, the neuronal stimulus is an applied voltage or current; in a photomemristor, it is a light pulse. The synaptic weight is encoded in the device's conductance or optical properties. Network connections are realized through crossbar lines or optical waveguides, mimicking axons and dendrites. The objective remains an engineering-focused implementation of analog storage and signal modulation for accelerated brain-inspired computing.

Table 2. Comparison of thin film memristor and photomemristor characteristics.

Characteristics	**Thin film memristor**	**Photomemristor**
Control signal	Electrical voltage	Light (intensity, wavelength, duration)
The nature of the response	Current (conductivity)	Optical (transmission, reflection, phase)
Nonlinearity/hysteresis	Current vs Voltage	Power vs Transmission
Physical mechanism	Ion migration, defect switching	Phase transition, photoconductivity, LSPR
Switching speed	~ns–mcs	~ps–ns
Switching energy	1–100 nJ	1–100 pJ
Number of analog states	2–64 (in the best cases >100)	8–32 (demonstrated), potential >100

3.3. Optical weighting elements based on microresonators, Mach–Zehnder interferometers (MZIs), and wavelength-division multiplexing (WDM) systems

Extending the analogy of memristors as artificial synapses to the optical domain, photonic neuromorphic systems require components that can controllably attenuate, delay, and route light to represent synaptic weights. Three principal architectures serve this function: Mach–Zehnder interferometers (MZIs), optical microresonators, and wavelength-division multiplexing (WDM) systems. They modulate an optical signal's phase or amplitude—functioning as a tunable weight—through refractive index changes driven by external stimuli such as voltage (in electro-optic, thermo-optic modulators) or a control-light intensity (in nonlinear devices).

The operational parameters of these elements vary by design. Required control power typically ranges from 0.1 to 10 mW, depending on material nonlinearity, with output signal power between −20 dB and 0 dB relative to input. Microresonators achieve quality factors (Q) of 10^4–10^6, defining their filtering sharpness. MZIs enable continuous 0 to 2π phase shifts with 1–10 V control voltages. Device footprints are compact (10–100 μm), with operational bandwidths of 10–100 GHz, enabling dense on-chip integration.

Although serving a common purpose, these architectures rely on distinct physical principles and thus require different mathematical descriptions. While approximate transfer functions relate output to control parameters under static conditions, a complete description demands fundamental models: Maxwell's equations with boundary conditions for resonators and waveguides, wave equations for MZIs, and spectral response functions for WDM multiplexers. These models are essential to capture dynamics, dissipation, and nonlinear effects absent in simple transfer functions.

The MZI transfer function is derived from the principle of linear interference between two optical paths with a controllable phase shift $\Delta\phi$ [119]:

$$\begin{aligned} I_{out} &= I_{in} \cos\left(\frac{\Delta\phi}{2}\right), \\ \Delta\phi &= \frac{2\pi}{\lambda} \Delta n L, \end{aligned} \tag{3.4}$$

where I_{out} is the output intensity, Δn is the change in the refractive index, and L is the length of the modulating section.

Input light is divided into two arms, propagates along them with distinct optical path lengths, and is recombined at the output. Depending on the relative phase difference, interference may be constructive or destructive, thereby controlling the transmitted intensity. In Eq. (3.4), modulation of the refractive index (e.g., via thermo-optic or electro-optic effects) enables precise control of the optical phase and, consequently, the output intensity. This makes the MZI a convenient and widely adopted building block for implementing tunable optical weights in neuromorphic photonic networks.

Microresonators, such as ring resonators, operate on the principle of resonant filtering, where light repeatedly circulates within a closed optical path. At specific wavelengths, constructive interference enhances the intracavity field, giving rise to sharp resonance peaks (or dips) in the transmission spectrum. These resonances are determined by the geometry and material properties of the resonator described by the wavelength-dependent transfer function $T(\lambda)$ of the microresonator:

$$T(\lambda) = \frac{1 - a^2}{1 - 2a\cos\theta + a^2}, \tag{3.5}$$

where a denotes the amplitude coupling (or loss) coefficient, and θ is the round-trip phase shift defined as

$$\theta = \frac{2\pi n_{\text{eff}} L}{\lambda}. \tag{3.6}$$

Here, n_{eff} is the effective refractive index, and L is the ring circumference. In this formulation, $T(\lambda)$ can be derived from the circulating field amplitude in the the full dynamical model given by Eq. (2.2), which represents a steady-state solution and captures the frequency response of the system under fixed control parameters. Weight modulation is achieved by tuning n_{eff} or a (e.g., via thermo-optic effects), thereby shifting the resonance wavelength or adjusting the filtering depth. Thus, microresonators act as optical weighting elements, modulating signal intensity through spectral selectivity and phase control.

Wavelength-division multiplexing (WDM) exploits this spectral selectivity to implement multichannel architectures. In WDM systems, each channel is addressed by a distinct wavelength, typically realized using arrays of microresonators tuned to different resonances or by diffraction gratings that provide spatial wavelength separation. Their behavior can be described by a matrix transfer function T, in which each element T_{ij} corresponds to the contribution of input channel i to output channel j:

$$T_i(\lambda) = \frac{1}{1 + \left(\frac{\lambda - \lambda_i}{\Delta\lambda_i}\right)^2}, \tag{3.7}$$

enabling compact description of large-scale, multi-wavelength systems such as WDM multiplexers.

The progression of these systems is illustrated by several representative studies. Initial work by [120] marked a conceptual transition from holographic implementations in photosensitive crystals to integrated chip-scale devices based on microresonators and phase-change materials, unifying these under the term "optical synapse". Subsequent development of WDM-based synapses utilizing microresonators and electro-absorption modulators [121] demonstrated a hybrid approach where a photodetected optical signal (0.01–50 mW) drove nonlinear opto-electro-optic (O–E–O) activation.

A significant advance came with the realization of all-optical activation functions in plasmon–exciton nanostructures (MNPs+QDs) and C_{60} [122], which achieved MNIST classification accuracies comparable to ReLU and sigmoid functions while operating with picosecond response times.

Concurrently, recurrent architectures were explored, with [123] demonstrating a GRU-like all-optical recurrent network using an SOA–MZI and fiber loop (~305 ns), which achieved an F1-score of 41.85% on the FI-2010 dataset at an energy cost of ∼180–300 pJ per symbol.

A central research direction has focused on enhancing programmability and robustness. This includes the on-chip training of an MZI array via a genetic algorithm [124], yielding ~94% accuracy on Iris classification with inherent noise tolerance. Scalability and resilience were further analyzed by [125], showing that 3-MZI and MZI+X configurations could maintain > 95% MNIST accuracy under phase noise ($\sigma = 0.1$ rad). The feasibility of *in situ* training was experimentally confirmed on 4×4 MZI chips using local optimization rules [126, 127], reducing matrix tuning errors below 1% within tens of iterations. A hardware–algorithm co-design approach presented in [128] employed gradient-free training on a 4×4 MZI chip to deliver ~90% classification accuracy, with numerical validation via tensor-train decomposition confirming scalability to 16×16 matrices.

Beyond large-scale interferometric networks, research has expanded toward novel materials and minimalist device designs. For instance, integrating phase-change materials with N-SiN MZIs enabled high extinction ratios up to 11 dB with low loss in the crystalline state [129]. Coherent processing architectures were demonstrated to handle 1 GHz spike streams of 130 ps duration while enabling dynamic weight control [130]. High-speed synaptic functionality was advanced through an SOA-REAM receiver capable of signed spike-train summation at 10 Gb/s [131], and programmable 4×4 MZI arrays were proposed for trainable matrix transformations [132]. Temporal processing was further exemplified by a photonic recurrent neuron using a 305 ns optical loop to classify 100 ps pulses at 10 Gb/s with over 91% accuracy [133].

Addressing critical challenges of non-volatile memory and fast reconfiguration, an ultralow-energy III–V/Si device (0.15–0.36 pJ, 300–900 ps) demonstrated power-free weight retention [134], while rapid switching was achieved with a 1×4 electro-optic switch featuring 20 ps operation and ≥25 dB extinction [135]. Practical system integration was supported by data-driven calibration techniques for MZI multipliers, where a neural-network model reduced the RMSE to 1.6 dB and facilitated scaling to 100 channels [136]. This trajectory culminated in the demonstration of the first all-optical ReLU neuron, which achieved 90% accuracy on Iris classification at 1 Gb/s [137].

Collectively, these works underscore progress driven by synergistic advances in materials (e.g., PCMs, III–V/Si) and the development of ultrafast, energy-efficient photonic components, paving the way for scalable neuromorphic platforms.

The concept of the optical synapse, now widely adopted in engineering-focused neuromorphic photonics, remains a conditional analogy to its biological counterpart. In contrast to biological synapses, typical optical implementations often lack distinct pre- and postsynaptic terminals, and the "neuron" function is commonly assigned to an external laser source without intrinsic neural dynamics. Furthermore, optical circuits are inherently symmetric and reversible, whereas biological synapses are strictly unidirectional. Direct optical interactions between neurons are not found in biology, except in photoreception (where light is an external stimulus) or optogenetics (where light serves as a control signal but neural communication remains electrochemical). Therefore, the term "optical synapse" is best interpreted as an engineering metaphor, describing a tunable optical channel rather than a strict biological replica.

Notwithstanding these conceptual distinctions, engineered optical synapses exhibit exceptional properties. They combine scalability, ultralow energy consumption, and multilevel plasticity, and they allow the co-integration of memory and processing within a single photonic component. These attributes represent a fundamental departure from conventional digital architectures and underscore the potential of neuromorphic photonics as a route to energy-efficient, high-performance computing.

3.4. Metasurface-based spatial light modulators

An emerging paradigm for optical weighting leverages metasurfaces—ultrathin, planar arrays of subwavelength optical elements that provide unprecedented control over the phase, amplitude, and polarization of light. In contrast to interferometric or resonant devices that operate in the temporal or spectral domain, metasurfaces enable direct spatial encoding of optical fields. This capability makes them exceptionally well-suited for massively parallel operations, such as optical convolution and matrix multiplication, by applying a spatially variant transfer function to an incident wavefront.

(i) Spatial beam shaping and optical weighting.

The operation of a metasurface can be described by a spatially dependent transmission (or reflection) function $T(x, y, \omega)$, which modulates an input optical field E_{in} to produce the output field E_{out}:

$$E_{\text{out}}(x, y, \omega) = T(x, y, \omega) \cdot E_{\text{in}}(x, y, \omega), \tag{3.8}$$

where the complex transfer function incorporates both amplitude and phase modulation:

$$T(x, y, \omega) = A(x, y, \omega) \cdot e^{i\Phi(x,y,\omega)}. \tag{3.9}$$

Here, $A(x, y, \omega)$ and $\Phi(x, y, \omega)$ represent the spatially encoded amplitude and phase profiles, respectively. This formulation allows a single static metasurface to implement a fixed, passive weighting matrix.

(ii) Spectral and polarization control.

For neuromorphic applications, dynamic reconfigurability is essential. This is achieved by integrating metasurfaces with active materials, including phase-change materials (e.g., GST, VO_2) [138], liquid crystals [139], and electrically tunable plasmonic elements [140]. Recent experimental demonstrations highlight the versatility of this approach:

- Reconfigurable metasurface modulators with switching times ranging from $\sim$ 0.7 ps to $\sim$ 7 μs and handling peak powers up to ~70 W [141].
- Holographic pattern generation for simultaneous multi-site optogenetic stimulation [142].
- All-optical matrix multiplication units with footprints below 100 μm^2 [143].

In this context, metasurfaces function as programmable spectral–polarization filters or multiplexing elements interfaced with WDM photonic systems.

The principal advantage of metasurfaces is their ability to implement spatially distributed synaptic weights in a single, compact layer, thereby avoiding the cumulative delay and insertion loss inherent in cascaded waveguide architectures. However, several challenges remain for their widespread adoption: (i) reconfiguration speeds are generally slower than those of electro-optic Mach–Zehnder interferometers; (ii) active metasurfaces often exhibit non-negligible insertion loss; and (iii) fabrication complexity escalates for large-scale, high-precision arrays.

(iii) Local field enhancement and light-matter interaction engineering.

A particularly compelling application lies at the intersection of neuromorphic photonics and neurotechnology, where metasurfaces provide both spatial field shaping and local field enhancement for optogenetic stimulation. By dynamically encoding phase patterns $\Phi(x, y, t)$, reconfigurable metasurfaces can project arbitrary three-dimensional light distributions onto neural tissue with subcellular precision [144, 145]. The required phase mask is typically computed via algorithms such as Gerchberg–Saxton or through direct holographic encoding:

$$\Phi(x, y) = \arg\left(\iiint A_{\text{target}}(x', y', z') \cdot G(x, y, x', y', z')\, dx'\, dy'\, dz'\right), \tag{3.10}$$

where A_{target} is the desired 3D intensity pattern, and G is the optical propagation kernel. When combined with fast temporal modulation, this enables precise 4D light sculpting for advanced optogenetic platforms [146].

In summary, metasurface-based spatial light modulators occupy a complementary position in photonic-optogenetic systems, serving mainly as spatial and spectral front-end processors rather than dynamical neuron elements. While technical hurdles in speed, loss, and fabrication persist, their intrinsic suitability for parallel optical processing and direct interface with biological neural systems positions them as a highly promising platform for next-generation neuromorphic photonic and neuro-optical applications [147, 148].

4. Neural network based on lasers and related photonic architectures

Laser dynamics have emerged as a compelling foundation for neuromorphic photonics, capitalizing on the intrinsic nonlinearity of optical resonators to emulate fundamental neural functions: excitation, spiking, phase synchronization, and chaotic behavior. This approach integrates the physics of coherent light emission with neuromorphic computing principles, offering pathways to computational systems with exceptional temporal resolution and energy efficiency.

While electronic neuromorphic circuits typically operate at nanosecond timescales, and individual memristive elements achieve picosecond dynamics primarily at the device level, laser-based neurons can sustain stable picosecond-to-femtosecond responses. This capability positions photonic neural networks to perform computations at frequencies beyond the practical limits of conventional silicon electronics. By leveraging the natural instability modes and nonlinear interactions of laser systems, these architectures open new avenues for high-speed, low-power neuromorphic processing that exploits the unique temporal and coherence properties of light.

4.1. CO_2 laser as an early model of the optical neuron

The analogy between laser dynamics and neuronal activity was first highlighted by Arecchi et al. [149, 150]. They demonstrated that homoclinic chaos in a CO_2 laser with delayed feedback, where a trajectory departs from a saddle point and subsequently returns, resembles spiking behavior in neurons. Striking parallels were identified between the temporal patterns of laser output and neural action potentials. By linearizing the system around a stable focus and introducing spatial coupling terms, the field evolution can be expressed as [149]:

$$\frac{dx}{dt} = f(x) + \varepsilon \nabla^2 x, \tag{4.1}$$

where $x(r, t)$ represents the local field variable, $f(x)$ local nonlinearity (e.g., excitation/relaxation of a CO_2 laser), and ε the coupling strength between neighboring oscillators. This formulation (4.1) established a conceptual bridge between laser physics and neurodynamics: the local term $f(x)$ corresponds to the excitable dynamics of a neuron, while the diffusive coupling $\varepsilon\nabla^2 x$ emulates synaptic or spatial interactions within a neural population.

More broadly, these studies showed that the mathematical models and nonlinear dynamics governing lasers provide deep insights into neuronal excitability, synchronization, and information processing, and vice versa. Such insights have spurred advances in neuromorphic photonics, paving the way for optical computing technologies. Shared features include thresholds, transitions to spiking regimes, nonlinear responses, and the emergence of synchronization when multiple units are coupled. These observations suggested that homoclinic chaos in lasers could serve as a foundation for neuromorphic computing [151].

Building upon these classical studies, later research extended the analysis of excitable and bursting dynamics to other photonic platforms while maintaining conceptual continuity with CO_2-laser physics. For instance, Kelleher et al. [152] demonstrated two-color bursting oscillations in optically injected quantum-dot lasers, explicitly linking their behavior to the slow–fast dynamics first identified in CO_2 lasers with saturable absorbers. In both systems, the separation of timescales, between the fast photon intensity and the slow modulation variable (carrier inversion or thermal detuning), gives rise to alternating active and silent phases analogous to neuronal bursting.

4.2. Semiconductor lasers model of the optical neuron

Semiconductor lasers became a natural continuation of neuron-like laser studies, as they combine strong nonlinearity, fast carrier dynamics, and on-chip integrability [153]. Unlike bulky gas lasers, they feature subnanosecond relaxation times and can be electrically pumped, making them ideal for compact photonic neurons [154]. Their behavior, from relaxation oscillations to spiking and chaotic regimes, is described by the same rate-equation framework introduced in Eq. (4.1), but with carrier lifetimes and saturation mechanisms characteristic of semiconductor media, where the photon lifetime is typically in the range of 1–10 ps, the carrier lifetime 0.1–2 ns, and the gain saturation governed by carrier depletion in quantum wells. Figure 5 illustrates the physical mechanism of neuron-like excitability in a semiconductor laser with optical feedback.

Carrier injection modulates the gain region, while partial reflections at the cavity facets sustain the optical field. The interplay between gain saturation, cavity losses, and feedback delay leads to the injected optical or electrical current exceeding the lasing threshold and carriers being rapidly depleted in the gain region (green), thereby resulting in a short optical pulse — the optical analogue of a neuronal spike. The partially reflecting facets sustain the intracavity field, while cavity losses and the feedback loop (blue arrow) determine the recovery dynamics and refractory period.The bottom arrow emphasizes that the photon lifetime τ_p is much shorter than the carrier lifetime τ_s, a key condition for excitability $\tau_p \ll \tau_s$. The insets show the temporal profiles of the input current and the resulting output spike. Together, these elements demonstrate how fast photon dynamics combined with slower carrier recovery can reproduce the threshold-and-refractory behavior characteristic of biological neurons.

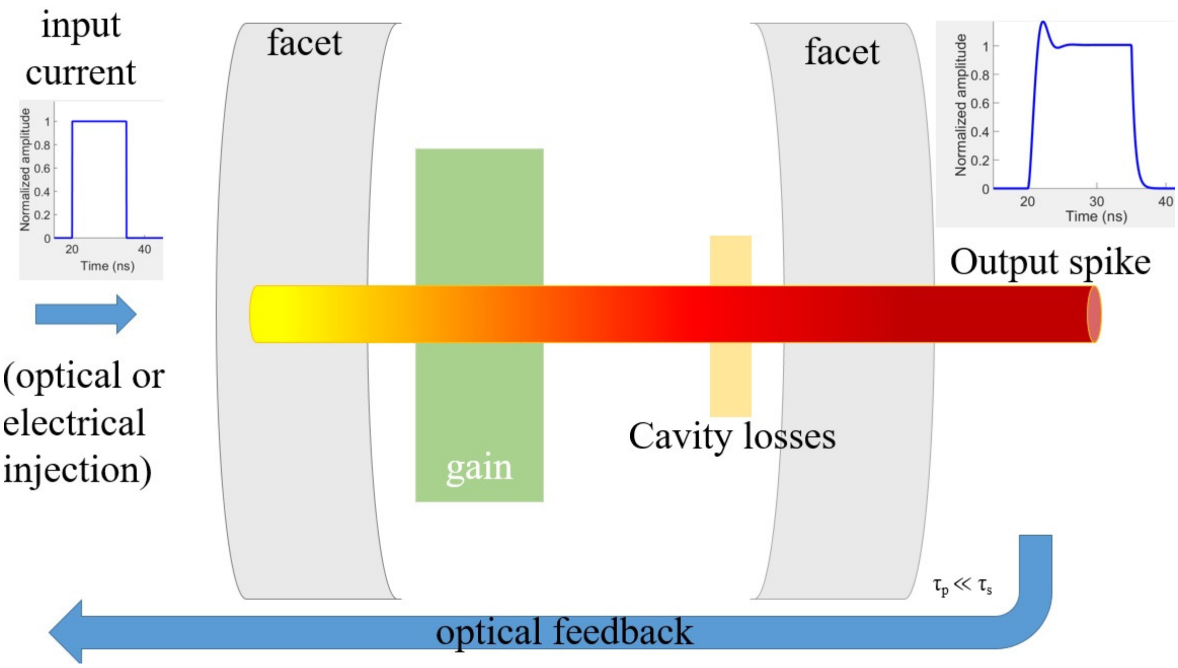

Figure 5. Schematic representation of neuron-like excitability in an edge-emitting semiconductor laser under optical or electrical injection.

Tiana-Alsina et al. [155] further demonstrated that semiconductor lasers respond to periodic forcing in a manner qualitatively similar to neurons, exhibiting spike-rate modulation dependent on both input amplitude and frequency. Comparable dynamics have since been observed across diverse laser systems, including fiber lasers [156] and integrated photonic devices [157], indicating a broader applicability of laser-based neuromorphic principles.

Early implementations relying on discrete semiconductor sources faced significant limitations in scalability and integration, constraining their practical deployment. Addressing these challenges, Prucnal et al. [158] systematically analyzed the dynamical similarities between semiconductor lasers and neurons, while highlighting vertical-cavity surface-emitting lasers (VCSELs) as particularly promising candidates for scalable network architectures.

4.3. VCSEL-based optical neuron model

The observation of neural-like dynamics was later extended to vertical-cavity surface-emitting lasers (VCSELs), where rich nonlinear behaviors, including spiking regimes and optical bistability, have been demonstrated [159–161]. Among various photonic neuron implementations, VCSEL-based systems are notably compact and technologically mature, accurately reproducing neuronal excitability through carrier–photon interactions. Their dual electrical and optical excitability allows them to function as direct, light-driven analogues of biological neurons—a conceptual parallel to optogenetics, albeit with a different physical mechanism. Collectively, these attributes position VCSELs and related photonic architectures as leading candidates for scalable, high-performance neuromorphic computing. It is important to note that photonic neural networks inherently form complex multi-loop feedback systems, where parameters such as coupling delays, detuning distributions, and gain dynamics govern overall stability, synchronization, and bifurcation structure.

VCSELs are particularly attractive for neuromorphic applications due to their compactness, low threshold currents, and inherent compatibility with photonic integration. Their dynamical response is governed by the interplay between carriers and photons, captured by the following rate equations:

$$\begin{aligned} \frac{dS}{dt} &= \left[G(N) - \frac{1}{\tau_p}\right] S + \beta \frac{N}{\tau_s}, \\ \frac{dN}{dt} &= \frac{I}{qV} - \frac{N}{\tau_s} - G(N)S, \end{aligned} \tag{4.2}$$

where S is the photon density, N the carrier density, τ_p and τ_s the photon and carrier lifetimes, $G(N)$ the optical gain, β the spontaneous emission factor, I the injection current, q the electron charge, and V the active volume.

A transient increase in the injection current raises the carrier density N above the lasing threshold, triggering a rapid, spike-like response in the photon density S. This excitability originates from the separation of timescales ($\tau_s \gg \tau_p$), where the fast photon dynamics produce the spike, while the slower carrier recovery defines the refractory period. This fast–slow structure closely mirrors classical neural models and aligns with the dynamical principles of other excitable photonic systems, such as the Fabry–Pérot saturable absorber neuron described by Eq. (2.3).

A series of experimental studies has successfully implemented artificial neurons using optoelectronic circuits pairing VCSELs with single-photon avalanche photodiodes [151, 159–161]. These systems reproduce hallmark features of biological neurons, including threshold behavior, all-or-nothing spiking, absolute refractory periods, and stimulus-dependent firing rates. By varying the duration of the optical excitation pulses, such neurons can support both temporal and rate coding schemes. Furthermore, adjusting the pulse amplitude allows operation in deterministic or probabilistic regimes, and stochastic resonance effects have been investigated to enhance signal detection.

Advancing from single-neuron operation to functional networks requires structured interconnectivity and control. Reservoir computing (RC) offers a powerful framework for both processing information and dynamically analyzing the collective behavior of such optoelectronic networks.

Figure 6 illustrates a VCSEL–SPAD reservoir computing network, conceptually extending the excitable optoelectronic neuron demonstrated by Chizhevsky et al. [159] into a recurrent photonic architecture. The system comprises three functional layers: an input layer for injecting optical or electrical stimuli, a central reservoir layer that performs nonlinear, transient signal processing via excitable dynamics, and a readout layer that linearly combines reservoir states to generate an output.

The fundamental unit, shown in Figure 6, is an artificial neuron built from an arbitrary function generator (AFG), a VCSEL, a variable optical attenuator (VOA), a single-photon avalanche diode (SPAD), and a monitoring photodiode (PD). In operation, the AFG drive signal is converted into an optical pulse by the VCSEL. This pulse is split: one path goes to the monitoring PD, while the other passes through the VOA to the SPAD. The SPAD acts as a threshold element, producing a digital output pulse only when the incident optical power exceeds its sensitivity, thereby emulating the all-or-none spiking behavior of a biological neuron. A local feedback loop from the SPAD output to the AFG input creates an inhibitory or refractory period, defining the neuron's excitability and recovery time. The combination of deterministic VCSEL carrier–photon dynamics (governed by rate equations like Eq. (4.2)) and the stochastic thresholding of the SPAD successfully reproduces key neuronal features, including threshold activation, a refractory period, and stereotyped spike output.

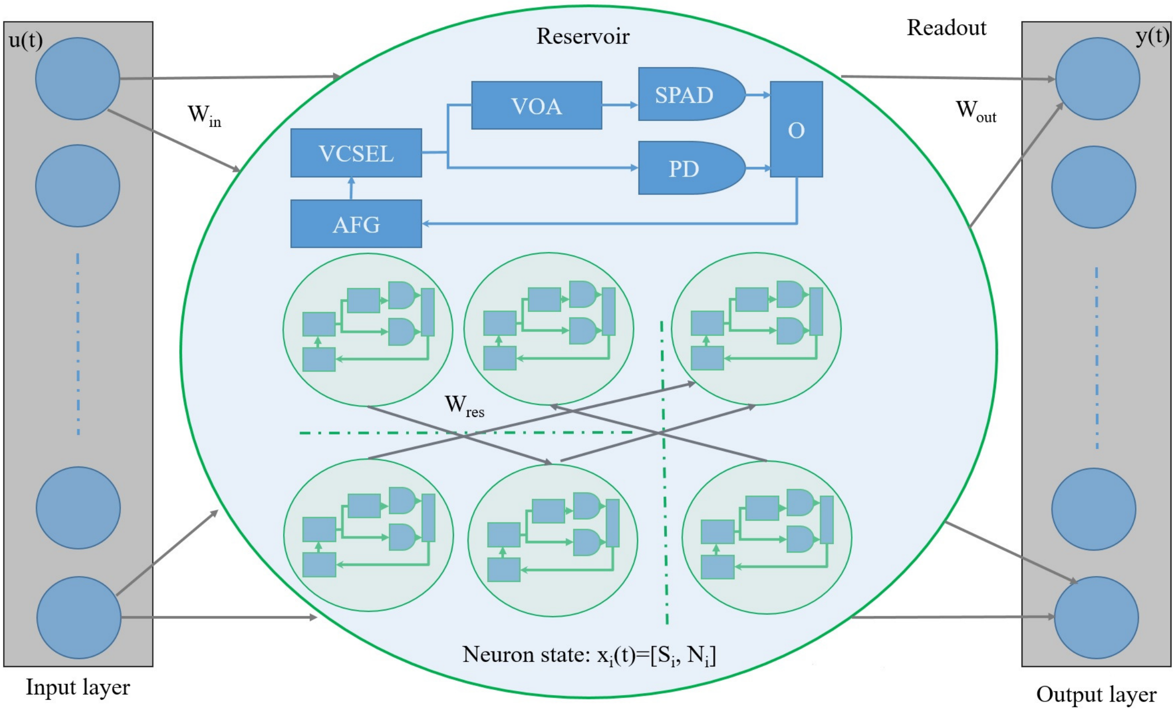

Figure 6. Schematic of a single optoelectronic neuron based on the experimental configuration showing the VCSEL–SPAD coupling with local feedback that reproduces neuron-like excitability. Reservoir layer is composed of multiple VCSEL–SPAD neurons interconnected through optical and electrical feedback pathways. Input and output layers provide signal injection and readout from the optical reservoir, respectively.

The reservoir layer is formed by interconnecting an array of these VCSEL–SPAD neurons through optical or electrical links. The collective state of the reservoir, denoted $\mathbf{x}(t)$, can be represented by the optical intensities $S_i(t)$ or the spiking events of each neuron i. Input stimuli $u(t)$ are coupled into the reservoir via an input weight matrix $\mathbf{W}_{\text{in}}$. Internally, neurons interact through delayed recurrent connections characterized by a weight matrix $\mathbf{W}_{\text{res}}$, where delays in Δt account for signal propagation and detector response times.

Finally, the readout layer samples the activity of selected reservoir neurons (e.g., via SPAD outputs or monitored PD signals) and applies a linear weight matrix $\mathbf{W}_{\text{out}}$ to produce the final, task-dependent output $y(t)$. Restricting learning to the readout layer has important implications for closed-loop biophotonic systems. Since the internal photonic dynamics remain fixed, the photonic substrate can provide a stable nonlinear transformation of neural signals, while adaptation occurs only at the interface to biological activity. This separation facilitates co-adaptation between photonic processing and evolving neural dynamics, as readout weights can be continuously updated without perturbing the underlying photonic hardware. As a result, readout-level training naturally supports robust closed-loop optogenetic control, where stimulation waveforms are adjusted in response to measured neural states.

In compact form, the network's dynamics can be described by the system:

$$\begin{aligned} \frac{d\mathbf{x}}{dt} &= \mathbf{F}(\mathbf{x}(t)) + \mathbf{W}_{\text{res}}\,\mathbf{x}(t-\Delta t) + \mathbf{W}_{\text{in}}\,u(t), \\ y(t) &= \mathbf{W}_{\text{out}}\,\mathbf{x}(t), \end{aligned} \tag{4.3}$$

where the nonlinear function **F** encapsulates the local excitable dynamics—thresholding, spike generation, and refractory behavior—of each individual VCSEL–SPAD neuron. This framework presents a pathway for implementing physical reservoir computing using scalable, neuromorphic photonic components.

Further extending the utility of photonic architectures for network-level analysis, Banerjee et al. [162] demonstrated that delay-coupled optoelectronic oscillators can successfully recover underlying network topology, even in the presence of noise and heterogeneous delays. These findings confirm that elementary photonic nodes, including VCSELs and Fabry–Pérot saturable absorbers, can be effectively analyzed and reconstructed at the network scale using RC methodologies.

Beyond spiking neurons, graded photonic neurons have attracted significant interest. These systems preserve the essential nonlinearity and excitability of their spiking counterparts but operate without a refractory period, enabling continuous response. For instance, Nie et al. [157] reported an integrated on-chip quantum-dot laser that functions as a graded neuron, achieving processing rates up to 10 Gbaud, offering a memory window of $\approx$ 1 ns, and performing reservoir computing without the need for delayed feedback. This illustrates how excitability can be harnessed for ultrafast, continuous signal processing.

Significant progress is also being made toward large-scale, trainable optical neural networks. Skalli et al. [163] demonstrated a model-free, end-to-end trained VCSEL-based optical neural network scalable to thousands of neurons with GHz inference bandwidth. This represents a critical transition from fixed-weight reservoir systems toward autonomous optical networks capable of in situ learning. Despite these advances, core challenges in scaling, system integration, and energy efficiency remain active areas of research [164–166].

To provide a unified dynamical comparison across prominent photonic neuron classes, including passive microresonators, Fabry–Pérot saturable absorber (FP–SA) lasers, and VCSEL-based neurons, we performed canonical time-domain simulations (Figure 7) using normalized, device-independent forms of Eqs. (2.1), (2.3), and (4.2). Our goal was to highlight the universal dynamical motifs shared across these physically distinct platforms.

All simulations were performed in normalized units using a Runge–Kutta 45 solver on an identical temporal grid (0–50, 5000 points). Initial conditions were set to zero. The input excitation consisted of a Gaussian pulse with an amplitude of 1.2 and a width of 0.5. This base signal was extended to explore different regimes: it was applied singly to probe excitability, duplicated with a 4-unit separation to test refractory behavior, combined with a continuous-wave step input of 0.6 to compare pulse and sustained responses, and incorporated into a delayed feedback loop (delay 3.0, coefficient 0.3) to study recurrent dynamics.

Model-specific parameters were chosen to operate each system in its excitable regime. For the passive microresonator (Eq. (2.1)), normalized loss and coupling coefficients were set to 1 and 2, respectively. For the Fabry–Pérot saturable absorber (FP–SA) laser neuron (Eq. (2.3)), the carrier pump rate was 0.2 with unity decay constants. For the VCSEL model (Eq. (4.2)), the normalized pump was set to 0.15, also with unity decay coefficients, and time was rescaled by the carrier lifetime.

The results, compiled in Figure 7, illustrate canonical dynamical regimes—excitability, refractoriness, response to sustained input, and delayed-feedback dynamics. Despite the distinct physical implementations of a passive resonator, an FP–SA laser, and a VCSEL, their simulated responses exhibit qualitatively similar nonlinear structures. This robust emergence of threshold activation, stereotyped

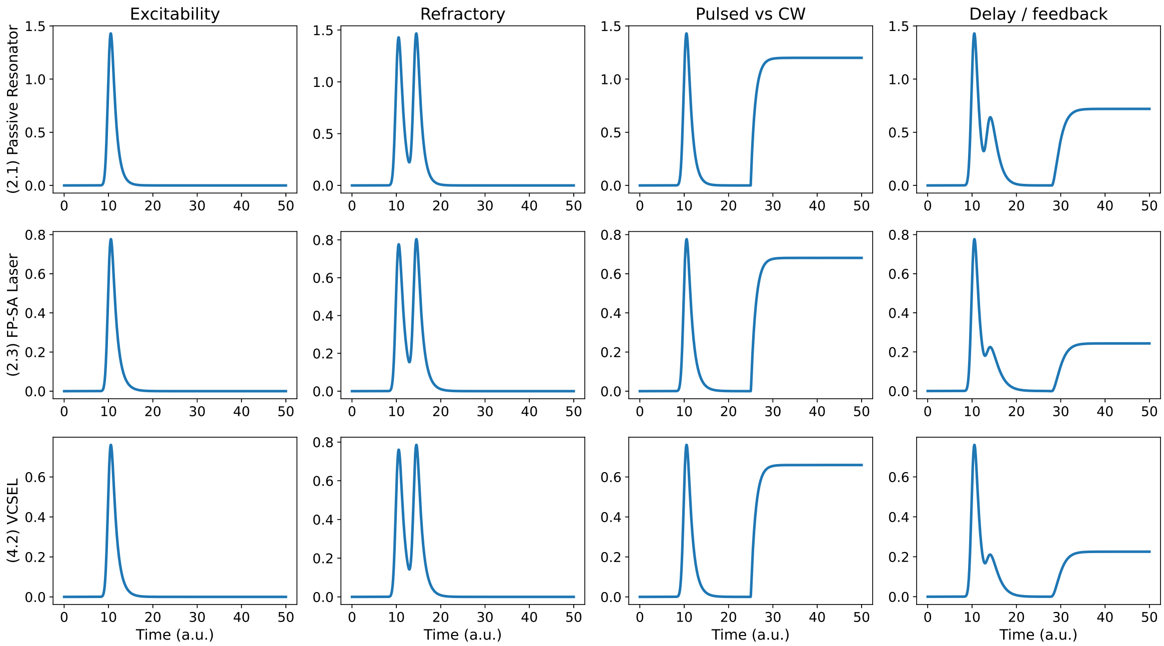

Figure 7. Simulated time series of three canonical photonic neuron models under various excitation conditions, highlighting their shared dynamical motifs. The three rows correspond to: (i) a passive microresonator (governed by Eq. (2.1)), (ii) a Fabry–Pérot saturable absorber (FP–SA) laser neuron (Eq. (2.3)), and (iii) a VCSEL-based neuron (Eq. (4.2)). The four columns illustrate distinct dynamical regimes: (a) Excitability: the system's response to a single suprathreshold pulse; (b) refractory behavior: the response to two successive pulses separated by an interval of 4 normalized time units, showing suppressed spiking during recovery; (c) pulsed vs. continuous-wave (CW) excitation: a comparison of the responses to a transient pulse and a sustained step input; and (d) delayed-feedback regime: dynamics under feedback with a delay of 3 normalized time units and a coupling coefficient of 0.3. These regimes correspond to biological excitability, refractory behavior, tonic firing, and recurrent neural dynamics commonly observed in optogenetically driven circuits.

spiking, and recovery periods across diverse photonic platforms demonstrates that the excitable behavior central to neuromorphic photonics is governed by universal nonlinear dynamical principles, rather than being specific to a particular material system or device architecture.

5. Conclusions

Over the past decade, photonic neural networks have matured into a highly promising platform for energy-efficient, high-speed computing. Beyond their clear potential to accelerate artificial intelligence, these systems uniquely enable the modeling and manipulation of biological neural processes. The convergence of photonics with optogenetics has been particularly impactful, establishing a natural framework for using light to probe and modulate neural activity, thereby positioning photonic architectures as powerful tools for both emulating and interfacing with neurobiological dynamics.

The integration of biologically plausible mechanisms, such as spike-timing-dependent coding, synaptic plasticity, and excitability governed by fast–slow dynamics, has significantly enhanced the realism and versatility of neuromorphic photonic systems. By aligning their operational principles with the functional characteristics of biological neurons, these platforms serve a dual purpose: as high-performance computational accelerators and as experimental testbeds for investigating neural phenomena. This dual capability supports the simulation of optogenetic experiments, the optimization of neuroprosthetic interfaces, and the development of hybrid systems for real-time interaction with neural tissues.

Looking ahead, several synergistic research vectors are critical for advancing the field:

- Large-scale integration and scalability: Developing dense, fully integrated photonic circuits with hundreds to thousands of neurons is essential for realizing complex, brain-inspired architectures.
- Hybrid photonic–electronic learning: Combining the high-speed parallelism of photonics with adaptive electronic control or on-chip training algorithms will enable fully trainable, large-scale networks with real-time learning capabilities.
- Enhanced biological fidelity: Incorporating more detailed neuronal and synaptic models, including dendritic processing and neuromodulatory feedback, will improve the realism and predictive power of optical neuromorphic simulations.
- Bio-interfaced systems: Directly coupling photonic circuits with living neural tissue or organoids could create transformative, closed-loop platforms for neurophysiological studies and therapeutic intervention.
- Reservoir computing and temporal processing: Exploiting the intrinsic dynamics of photonic systems for temporal coding and memory offers a direct path to ultra-fast, brain-inspired information processing.
- Energy efficiency and robustness: Optimizing device design, network architectures, and noise tolerance remains paramount for the practical deployment of photonic neural systems in real-world applications.

A critical frontier is the development of a complete closed-loop optogenetic interface, which requires integrated photonic components for both writing (stimulation) and reading (sensing) neural activity, coupled with neuromorphic processing for real-time adaptation. Emerging technologies, such as optoelectronic synaptic transistors based on organic semiconductors [167, 168], provide this essential bidirectional link. These devices function as biorealistic, tunable synaptic elements that transduce optical readout signals into adaptive electronic responses, enabling on-chip learning and dynamic modulation of optical stimulation. This synergy points toward fully autonomous, intelligent neuromodulation systems.

From a system-level perspective, photonic neurons and optogenetic interfaces act as co-located actuators and sensors within hybrid neural systems. Their performance must be evaluated through rigorous metrics of stability, robustness to parameter drift, and resilience to measurement noise. While this engineering-driven approach, which often combines weighting, memory, and activation within a single photonic element, may reduce strict biological modularity, it offers distinct advantages in scalability and energy efficiency. Consequently, training and inference in these systems rely on principles of programmability and device-level reconfigurability, diverging from, yet complementing, biological network organization.

In summary, neurophotonics integrates photonics, neuroscience, and computation to forge a unique interdisciplinary pathway. By merging classical optical nonlinearities with bio-inspired and optogenetic strategies, it enables systems that are fundamentally efficient, high-speed, and adaptive. Sustained progress in this arena promises not only to accelerate the development of powerful neuromorphic computing but also to revolutionize our understanding of the brain and pioneer new frontiers in medical diagnostics and therapeutics.

Use of AI tools declaration

The authors declare they have not used Artificial Intelligence (AI) tools in the creation of this article.

Acknowledgments

The study is supported by the Ministry of Science and Higher Education of Russian Federation (contract # FSWR-2020-0036).

Conflict of interest

The authors declare there is no conflict of interest. Prof. Alexander N. Pisarchik is an special issue editor for Mathematical Biosciences and Engineering and was not involved inthe editorial review or the decision to publish this article.

References

1. E. S. Boyden, F. Zhang, E. Bamberg, G. Nagel, K. Deisseroth, Millisecond-timescale, genetically targeted optical control of neural activity, *Nat. Neurosci.*, **8** (2005), 1263–1268. https://doi.org/10.1038/nn1525
2. K. Deisseroth, Optogenetics, *Nat. Methods*, **8** (2011), 26–29. https://doi.org/10.1038/nmeth.f.324
3. L. Fenno, O. Yizhar, K. Deisseroth, The development and application of optogenetics, *Annu. Rev. Neurosci.*, **34** (2011), 389–412. https://doi.org/10.1146/annurev-neuro-061010-113817
4. M. Häusser, Optogenetics: The age of light, *Nat. Methods*, **11** (2014), 1012–1014. https://doi.org/10.1038/nmeth.3111
5. B. R. Rost, J. Wietek, O. Yizhar, D. Schmitz, Optogenetics at the presynapse, *Nat. Neurosci.*, **25** (2022), 984–998. https://doi.org/10.1038/s41593-022-01113-6
6. A. Armbruster, A. M. Mohamed, H. T. Phan, W. Weber, Lighting the way: Recent developments and applications in molecular optogenetics, *Curr. Opin. Biotechnol.*, **87** (2024), 103126. https://doi.org/10.1016/j.copbio.2024.103126
7. V. S. Ovechkina, S. K. Andrianova, I. O. Shimanskaia, P. S. Suvorova, A. Y. Ryabinina, M. L. Blagonravov, et al., Advances in optogenetics and thermogenetics for control of non-neuronal cells and tissues in biomedical research, *ACS Chem. Biol.*, **20** (2025), 553–572. https://doi.org/10.1021/acschembio.4c00842
8. T. Kushibiki, Current topics of optogenetics for medical applications toward therapy, in: *Optogenetics: Light-Sensing Proteins and Their Applications in Neuroscience and Beyond*, 2021, pp. 513–521. https://doi.org/10.1007/978-981-15-8763-4_35

9. Y. Zhou, Y. Wei, L. Li, T. Yan, H. Ye, Optogenetics in medicine: Innovations and therapeutic applications, *Curr. Opin. Biotechnol.*, **92** (2025), 103262. https://doi.org/10.1016/j.copbio.2025.103262
10. A. M. Packer, B. Roska, M. Häusser, Targeting neurons and photons for optogenetics, *Nat. Neurosci.*, **16** (2013), 805–815. https://doi.org/10.1038/nn.3427
11. C. Belzung, M. Turiault, G. Griebel, Optogenetics to study the circuits of fear- and depression-like behaviors: a critical analysis, *Pharmacol. Biochem. Behav.*, **122** (2014), 144–157. https://doi.org/10.1016/j.pbb.2014.04.002
12. V. Emiliani, A. E. Cohen, K. Deisseroth, M. Häusser, All-optical interrogation of neural circuits, *J. Neurosci.*, **35** (2015), 13917–13926. https://doi.org/10.1523/JNEUROSCI.2916-15.2015
13. C. K. Kim, A. Adhikari, K. Deisseroth, Integration of optogenetics with complementary methodologies in systems neuroscience, *Nat. Rev. Neurosci.*, **18** (2017), 222–235. https://doi.org/10.1038/nrn.2017.15
14. S. Boccaletti, A. N. Pisarchik, C. I. del Genio, A. Amann, *Synchronization: From Coupled Systems to Complex Networks*, Cambridge University Press, Cambridge, 2018. https://doi.org/10.1017/9781107297111
15. A. N. Pisarchik, A. E. Hramov, *Multistability in Physical and Living Systems: Characterization and Applications*, Springer Nature, Cham, Switzerland, 2022. https://doi.org/10.1007/978-3-030-98396-3
16. R. FitzHugh, Impulses and physiological states in theoretical models of nerve membrane, *Biophys. J.*, **1** (1961), 445–466. https://doi.org/10.1016/S0006-3495(61)86902-6
17. S. A. Gerasimova, A. Beltyukova, A. Fedulina, M. Matveeva, A. V. Lebedeva, A. N. Pisarchik, Living-neuron-based autogenerator, *Sensors*, **23** (2023), 7016. https://doi.org/10.3390/s23167016
18. J. L. Hindmarsh, R. M. Rose, A model of neuronal bursting using three coupled first order differential equations, *Proc. R. Soc. Lond. B Biol. Sci.*, **221** (1984), 87–102. https://doi.org/10.1098/rspb.1984.0024
19. C. Koch, I. Segev, *Methods in Neuronal Modeling: From Ions to Networks*, MIT Press, Cambridge, 1998.
20. E. M. Izhikevich, *Dynamical Systems in Neuroscience: The Geometry of Excitability and Bursting*, MIT Press, Cambridge, 2007.
21. P. Dayan, L. F. Abbott, *Theoretical Neuroscience: Computational and Mathematical Modeling of Neural Systems*, MIT Press, Cambridge, 2005.
22. B. Ermentrout, D. H. Terman, *Mathematical Foundations of Neuroscience*, Springer, New York, 2010.
23. G. Arora, A. Rocha, S. Patta, Computational intelligence algorithms for the diagnosis of neurological disorders, in: *Navigating the Complexities of the Brain: Challenges and Opportunities in Computational Neurology*, 2026, pp. 18–30. https://doi.org/10.1201/9781003520344

24. S. Martinez, D. Garcia-Violini, M. Belluscio, J. Piriz, R. Sanchez-Pena, Dynamical models in neuroscience from a closed-loop control perspective, *IEEE Rev. Biomed. Eng.*, **16** (2022), 706–721. https://doi.org/10.1109/RBME.2022.3180559
25. S. Martínez, R. S. Sánchez-Peña, D. García-Violini, Controlling neural activity: LPV modelling of optogenetically actuated Wilson–Cowan model, *J. Neural Eng.*, **21** (2024), 036002. https://doi.org/10.1088/1741-2552/ad4212
26. Q. Guo, J. Zhou, Q. Feng, R. Lin, H. Gong, Q. Luo, et al., Multi-channel fiber photometry for population neuronal activity recording, *Biomed. Opt. Express*, **6** (2015), 3919–3931. https://doi.org/10.1364/BOE.6.003919
27. O. Rogozhnikova, M. Solotenkov, O. Ivashkina, I. Fedotov, A. Fedotov, K. Anokhin, Novel optical probe for multi-region fiber photometry in mouse brain, *2024 Sixth International Conference Neurotechnologies and Neurointerfaces (CNN)*, Kaliningrad, Russian Federation, 2024, pp. 171–174. https://doi.org/10.1109/CNN63506.2024.10705861
28. A. R. Freeda, R. Kanthavel, A. Anju, Scalability issues in AI computing in large-scale networks, in: *AI for Large Scale Communication Networks*, IGI Global, 2025, pp. 395–414. https://doi.org/10.4018/979-8-3693-6552-6.ch018
29. V. S. Bhargavi, N. M. Sawai, M. K. Chakravarthi, S. H. Ibrahim, L. A. Pérez, M. Tiwari, Scalability and performance of blockchain-based solutions for IoT applications, in: *Interdisciplinary Approaches to AI, Internet of Everything, and Machine Learning*, IGI Global, 2025, pp. 203–216.
30. T. Ferreira De Lima, B. J. Shastri, A. N. Tait, M. A. Nahmias, P. R. Prucnal, Progress in neuromorphic photonics, *Nanophotonics*, **6** (2017), 577–599. https://doi.org/10.1515/nanoph-2016-0139
31. B. J. Shastri, A. N. Tait, T. Ferreira de Lima, W. H. P. Pernice, H. Bhaskaran, C. D. Wright, et al., Photonics for artificial intelligence and neuromorphic computing, *Nat. Photonics*, **15** (2021), 102–114. https://doi.org/10.1038/s41566-020-00754-y
32. L. El Srouji, A. Krishnan, R. Ravichandran, Y. Lee, M. On, X. Xiao, et al., Photonic and optoelectronic neuromorphic computing, *APL Photonics*, **7** (2022), 051101. https://doi.org/10.1063/5.0072090
33. T. Fu, J. Zhang, R. Sun, Y. Huang, W. Xu, S. Yang, et al., Optical neural networks: Progress and challenges, *Light Sci. Appl.*, **13** (2024), 263. https://doi.org/10.1038/s41377-024-01590-3
34. S. Song, J. Kim, S. M. Kwon, J.-W. Jo, S. K. Park, et al., Recent progress of optoelectronic and all-optical neuromorphic devices: A comprehensive review of device structures, materials, and applications, *Adv. Intell. Syst.*, **3** (2021), 2000119. https://doi.org/10.1002/aisy.202000119
35. K. Yang, J. J. Yang, R. Huang, Y. Yang, Nonlinearity in memristors for neuromorphic dynamic systems, *Small Sci.*, **2** (2022), 2100049. https://doi.org/10.1002/smsc.202100049
36. Z. Huo, Q. Sun, J. Yu, Y. Wei, Y. Wang, J. H. Cho, et al., Neuromorphic devices assisted by machine learning algorithms, *Int. J. Extrem. Manuf.*, **7** (2025), 042007. https://doi.org/10.1088/2631-7990/adba1e
37. J. Sun, J. Sun, X. Li, Y. Sun, Q. Hong, C. Wang, A review of recent developments in neuromorphic computing based on emerging memory devices, *Nonlinear Dyn.*, **133** (2025), 33035–33061. https://doi.org/10.1007/s11071-025-11727-7

38. R. George, M. Chiappalone, M. Giugliano, T. Levi, S. Vassanelli, J. Partzsch, et al., Plasticity and adaptation in neuromorphic biohybrid systems, *iScience*, **23** (2020), 101589. https://doi.org/10.1016/j.isci.2020.101589

39. B. J. Barros, J. P. S. Cunha, Neurophotonics: a comprehensive review, current challenges and future trends, *Front. Neurosci.*, **18** (2024), 1382341. https://doi.org/10.3389/fnins.2024.1382341

40. J. Yao, Y. Teng, Q. Wang, Y. He, L. Liu, C. Zhao, et al., Advancing intelligent neuromorphic computing: Recent progress in all-optical-controlled artificial synaptic devices, *ACS Nano*, **19** (2025), 26320–26346. https://doi.org/10.1021/acsnano.5c05240

41. R. Li, Y. Gong, H. Huang, Y. Zhou, S. Mao, Z. Wei, et al., Photonics for neuromorphic computing: Fundamentals, devices, and opportunities, *Adv. Mater.*, **37** (2025), 2312825. https://doi.org/10.1002/adma.202312825

42. C. Lüscher, V. Emiliani, N. Farahany, A. Gittis, V. Gradinaru, K. A. High, et al., Roadmap for direct and indirect translation of optogenetics into discoveries and therapies for humans, *Nat. Neurosci.*, (2025), 1–17. https://doi.org/10.1038/s41593-025-02097-9

43. G. P. Agrawal, *Nonlinear Fiber Optics*, 5th edition, Academic Press, Oxford, UK, 2007. https://doi.org/10.1007/3-540-46629-0_9

44. G. Khitrova, H. M. Gibbs, F. Jahnke, M. Kira, S. W. Koch, Nonlinear optics of normal-mode-coupling semiconductor microcavities, *Rev. Mod. Phys.*, **71** (1999), 1591–1639. https://doi.org/10.1103/RevModPhys.71.1591

45. K. J. Vahala, Optical microcavities, *Nature*, 424 (2003), 839–846. https://doi.org/10.1038/nature01939

46. J. Xiang, A. Torchy, X. Guo, Y. Su, All-optical spiking neuron based on passive microresonator, *J. Lightwave Technol.*, **38** (2020), 4019–4029. https://doi.org/10.1109/JLT.2020.2986233

47. Y. Yang, Y. Deng, X. Xiong, B. Shi, L. Ge, J. Wu, Neuron-like optical spiking generation based on silicon microcavity, in: *2020 IEEE 20th International Conference on Communication Technology (ICCT)*, 2020, pp. 970–974. https://doi.org/10.1109/ICCT50939.2020.9295847

48. S. Donati, *Photodetectors: Devices, Circuits and Applications*, John Wiley & Sons, 2021. https://doi.org/10.1088/0957-0233/12/5/703

49. B. J. G. Castro, C. Peucheret, D. Zibar, F. Da Ros, Impact of free-carrier nonlinearities on silicon microring-based reservoir computing, in: *IEEE Photonics Conference (IPC)*, 2023, pp. 1–2. https://doi.org/10.1109/IPC57732.2023.10360595

50. S. Biasi, A. Lugnan, D. Micheli, L. Pavesi, Exploring the potential of self-pulsing optical microresonators for spiking neural networks and sensing, *Commun. Phys.*, **7** (2024), 380. https://doi.org/10.1038/s42005-024-01869-2

51. D. Bazzanella, Microring based neuromorphic photonics, PhD Thesis, Université Paris-Saclay, 2022.

52. Y. Ye, Y. Xie, T. Song, N. Guan, M. Lv, C. Li, Integrated plasmonic full adder based on cascaded rectangular ring resonators for optical computing, *Opt. Laser Technol.*, **156** (2022), 108479. https://doi.org/10.1016/j.optlastec.2022.108479

53. X. Shen, R. C. Beltran, V. M. Diep, S. Soltani, A. M. Armani, Low-threshold parametric oscillation in organically modified microcavities, *Sci. Adv.*, **4** (2018), eaao4507. https://doi.org/10.1126/sciadv.aao4507
54. H. Yuan, Y. Xie, B. Liu, X. Jiang, J. Chai, Y. Ye, et al., Self-pulsation and synchronization of optical neurons based on microrings, *Opt. Laser Technol.*, **172** (2024), 110479. https://doi.org/10.1016/j.optlastec.2023.110479
55. J. Xiang, Y. Zhao Y, A. He, J. Xiao, Y. Su, X. Guo, Photonic neuromorphic processing with on-chip electrically-driven microring spiking neuron, *Laser Photon. Rev.*, **19** (2025), 2400604. https://doi.org/10.1002/lpor.202400604
56. M. Tamura, H. Morison, A. N. Tait, B. J. Shastri, Design of a monolithic silicon-on-insulator resonator spiking neuron, *Commun. Phys.*, **7** (2024), 303. https://doi.org/10.1038/s42005-024-01769-5
57. L. Xu, J. Zhang, E. A. Doris, S. Bilodeau, J. A. Wisch, M. Gui, et al., Building scalable silicon microring resonator-based neuromorphic photonic circuits using post-fabrication processing with photochromic material, *Adv. Opt. Mater.*, **13** (2025), 2402706. https://doi.org/10.1002/adom.202402706
58. S. Xiang, Y. Han Y, S. Gao, Z. Song, Y. Zhang, D. Zheng, et al., Semiconductor lasers for photonic neuromorphic computing and photonic spiking neural networks: A perspective, *APL Photon.*, **9** (2024), 070902. https://doi.org/10.1063/5.0217968
59. D. Zheng, S. Xiang, X. Guo, Y. Zhang, B. Gu, H. Wang, et al., Experimental demonstration of coherent photonic neural computing based on a Fabry–Perot laser with a saturable absorber, *Photon. Res.*, **11** (2022), 65–71. https://doi.org/10.1364/PRJ.471950
60. T. Fu, J. Zhang, R. Sun, Y. Huang Y, W. Xu, S. Yang, et al., Optical neural networks: Progress and challenges, *Light Sci. Appl.*, **13** (2024), 263. https://doi.org/10.1038/s41377-024-01590-3
61. Y. Shi, S. Xiang, X. Guo, Y. Zhang, H. Wang, D. Zheng, et al., Photonic integrated spiking neuron chip based on a self-pulsating DFB laser with a saturable absorber, *Photon. Res.*, **11** (2023), 1382–1389. https://doi.org/10.1364/PRJ.485941
62. Z. Song, S. Xiang, X. Guo, S. Gao, B. Gu, D. Zheng, et al., Nonlinear neural computation in an integrated FP-SA spiking neuron subject to incoherent dual-wavelength optical pulse injections, *Sci. China Inf. Sci.*, **66** (2023), 229405. https://doi.org/10.1007/s11432-022-3749-3
63. J. M. Barakat, A. S. Karar, R. Ghandour, Z. N. Gürkan, Advances in optical bistability: Theory, devices, and emerging applications, *Results Eng.*, (2025), 105540. https://doi.org/10.1016/j.rineng.2025.105540
64. H. Pezeshki, V. Ahmadi, All-optical bistable switching based on photonic crystal slab nanocavity using nonlinear Kerr effect, *J. Modern Opt.*, **60** (2013), 103–108. https://doi.org/10.1080/09500340.2012.737033
65. R. D. Hontinfinde, C. Z. Mamlankou, S. I. Hontinfinde, M. A. Ayela, G. Edah, Physics-informed neural networks for predicting ultrashort optical pulse dynamics in nonlinear fiber systems, *Optik*, (2026), 172673. https://doi.org/10.1016/j.ijleo.2026.172673

66. Z. Ye, A. Fülöp, O. B. Helgason, P. A. Andrekson, V. Torres-Company, Low-loss high-Q silicon-rich silicon nitride microresonators for Kerr nonlinear optics, *Opt. Lett.*, **44** (2019), 3326–3329. https://doi.org/10.1364/OL.44.003326

67. J. M. Silver, P. Del'Haye, Generalized theory of optical resonator and waveguide modes and their linear and Kerr nonlinear coupling *Phys. Rev. A*, **105** (2022), 023517. https://doi.org/10.1103/PhysRevA.105.023517

68. Y. Cai, X. Deng, L. Zhang, Z. Ni, J. Mai, P. Huang, at al., Quantum squeezing amplification with a weak Kerr nonlinear oscillator, *Nat. Commun.*, **17** (2025), 1–8. https://doi.org/10.1038/s41467-025-67699-0

69. S. T. Rizvi, L. Jlali, S. Riaz, A. R. Seadawy, Dispersion controlled vector quartic solitons on a continuous-wave background: Exact families and stability in coupled higher-order Schrödinger dynamic equation, *Eur. Phys. J. Plus*, **141** (2026), 11. https://doi.org/10.1140/epjp/s13360-025-07198-9

70. N. Accanto, F. G. Blot, A. Lorca-Cámara, V. Zampini, F. Bui, C. Tourain C, et al., A flexible two-photon fiberscope for fast activity imaging and precise optogenetic photostimulation of neurons in freely moving mice, *Neuron*, **111** (2023), 176–189. https://doi.org/10.1016/j.neuron.2022.10.030

71. A. Lorca-Cámara, C. Tourain, V. de Sars, V. Emiliani, N. Accanto N, Multicolor two-photon light-patterning microscope exploiting the spatio-temporal properties of a fiber bundle, *Biomed. Opt. Express*, **15** (2024), 2094–2109. https://doi.org/10.1364/BOE.507690

72. A. Lorca-Cámara, F. G. Blot, N. Accanto, Recent advances in light patterned optogenetic photostimulation in freely moving mice, *Neurophotonics*, **11** (2024), S11508. https://doi.org/10.1117/1.NPh.11.S1.S11508

73. Ya. I. Pigareva, O. O. Antipova, V. N. Kolpakov, O. V. Martynova, A. A. Popova, I. V. Mukhina, et al., A method for recording the bioelectrical activity of neural axons upon stimulation with short pulses of infrared laser radiation, *Sovrem. Tehnol. Med.*, **12** (2020), 21–27. https://doi.org/10.17691/stm2020.12.6.03

74. S. Jin, J. Li, L. Jiang, Y. Ye, C. Ma, Y. Yang, et al., Instant noninvasive near-infrared deep brain stimulation using optoelectronic nanoparticles without genetic modification, *Sci. Adv.*, **11** (2025), eadt4771. https://doi.org/110.1126/sciadv.adt4771

75. P. Abdollahian, K. Sui, G. Li, R. W. Berg, M. Meneghetti, C. Markos, Evaluating safe infrared neural stimulation parameters: Calcium dynamics and excitotoxicity thresholds in dorsal root ganglia neurons, *J. Neurosci. Methods*, (2025), 110484. https://doi.org/10.1016/j.jneumeth.2025.110484

76. M. Meneghetti, J. Kaur, K. Sui, J. F. Sørensen, R. W. Berg, C. Markos, Soft monolithic infrared neural interface for simultaneous neurostimulation and electrophysiology, *Light Sci. Appl.*, **12** (2023), 127. https://doi.org/10.1038/s41377-023-01164-9

77. G. Zhu, J. Xiong, X. Li, Z. He, S. Zhong, J. Chen, et al., Neural stimulation and modulation with sub-cellular precision by optomechanical bio-dart, *Light Sci. Appl.*, **13** (2024), 258. https://doi.org/10.1038/s41377-024-01617-9

78. R. W. Boyd, *Contemporary Nonlinear Optics*, Elsevier, 2012.

79. E. Papagiakoumou, Optical developments for optogenetics, *Biol. Cell*, **105** (2013), 443–464. https://doi.org/10.1111/boc.201200087

80. J. C. Williams, J. Xu, Z. Lu, A. Klimas, X. Chen, C. M. Ambrosi, et al., Computational optogenetics: empirically-derived voltage- and light-sensitive channelrhodopsin-2 model, *PLoS Comput. Biol.*, **9** (2013), e1003220. https://doi.org/10.1371/journal.pcbi.1003220

81. V. Renault, M. Thieullen, E. Trélat, Minimal time spiking in various ChR2-controlled neuron models, *J. Math. Biol.*, **76** (2018), 567–608. https://doi.org/10.1007/s00285-017-1101-1

82. B. D. Evans, S. Jarvis, S. R. Schultz, K. Nikolic, PyRhO: a multiscale optogenetics simulation platform, *Front. Neuroinform.*, **10** (2016), 8. https://doi.org/10.3389/fninf.2016.00008

83. S. A. Gerasimova, G. V. Gelikonov, A. N. Pisarchik, V. B. Kazantsev, Synchronization of optically coupled neural-like oscillators, *J. Commun. Technol. Electron.*, **60** (2015), 900–903. https://doi.org/10.1134/S1064226915070062

84. A. N. Pisarchik, R. Jaimes-Reátegui, J. R. Sevilla-Escoboza, J. H. García-Lopez, V. B. Kazantsev, Optical fiber synaptic sensor, *Opt. Lasers Eng.*, **49** (2011), 736–742. https://doi.org/10.1016/j.optlaseng.2011.01.020

85. A. N. Pisarchik, R. Jaimes-Reátegui, J. R. Sevilla-Escoboza, F. R. Ruiz-Oliveras, R. Flavio, J. H. García-López, Two-channel opto-electronic chaotic communication system, *J. Franklin Inst.*, **349** (2012), 3194–3202. https://doi.org/10.1016/j.jfranklin.2012.10.005

86. A. N. Pisarchik, J. R. Sevilla-Escoboza, R. Jaimes-Reátegui, G. Huerta-Cuellar, J. H. García-López, V. B. Kazantsev, Experimental implementation of a biometric laser synaptic sensor, *Sensors*, **13** (2013), 17322–17331. https://doi.org/10.3390/s131217322

87. R. R. Jaimes-Reátegui, J. M. Reyes-Estolano, J. H. García-López, G. Huerta-Cuellar, C. E. Rivera-Orozco, A. N. Pisarchik, Numerical study of laser synapse connecting Hindmarsh–Rose neurons, *Eur. Phys. J. Spec. Top.*, (2022), 1–10. https://doi.org/10.1140/epjs/s11734-021-00357-w

88. M. Xu, X. Mai, J. Lin, W. Zhang, Y. Li, Y. He, et al., Recent advances on neuromorphic devices based on chalcogenide phase-change materials, *Adv. Funct. Mater.*, **30** (2020), 2003419. https://doi.org/10.1002/adfm.202003419

89. O. Bichler, M. Suri, D. Querlioz, D. Vuillaume, B. DeSalvo, C. Gamrat, Visual pattern extraction using energy-efficient '2-PCM synapse' neuromorphic architecture, *IEEE Trans. Electron. Dev.*, **59** (2012), 2206–2214. https://doi.org/10.1109/TED.2012.2197951

90. Y. Demirağ, F. Moro, T. Dalgaty, G. Navarro, C. Frenkel, G. Indiveri, et al., PCM-trace: scalable synaptic eligibility traces with resistivity drift of phase-change materials, in: *2021 IEEE International Symposium on Circuits and Systems (ISCAS)*, 2021. https://doi.org/10.1109/ISCAS51556.2021.9401446

91. K. Aryana, H. J. Kim, C. C. Popescu, S. Vitale, H. B. Bae, T. Lee, et al., Toward accurate thermal modeling of phase change material-based photonic devices, *Small*, **19** (2023), 2304145. https://doi.org/10.1002/smll.202304145

92. K. Shportko, S. Kremers, M. Woda, D. Lencer, J. Robertson, M. Wuttig, Resonant bonding in crystalline phase-change materials, *Nat. Mater.*, **7** (2008), 653–658. https://doi.org/10.1038/nmat2226

93. J. Kalb, *Phase Change Materials: Science and Applications*, Springer, New York, 2014. https://doi.org/10.1007/978-0-387-84874-7_7

94. B. E. A. Saleh, M. C. Teich, *Fundamentals of Photonics*, 3rd edition, John Wiley & Sons, 2019.

95. V. V. Ionin, A. V. Kiselev, A. A. Burtsev, V. A. Mikhalevsky, N. N. Eliseev, I. M. Asharchuk, et al., An optical synapse based on a polymer waveguide with a GST225 active layer, *Appl. Phys. Lett.*, **119** (2021), 083301. https://doi.org/10.1063/5.0063349

96. Z. Cheng, C. Ríos, W. H. Pernice, C. D. Wright, H. Bhaskaran, On-chip photonic synapse, *Sci. Adv.*, **3** (2017), e1700160. https://doi.org/10.1126/sciadv.170016

97. A. H. A. Nohoji, P. Keshavarzi, M. Danaie, A photonic crystal waveguide intersection using phase change material for optical neuromorphic synapses, *Opt. Mater.*, **151** (2024), 115372. https://doi.org/10.1016/j.optmat.2024.115372

98. Y. Zhang, D. Yao, Y. Liu, C. Fang, S. Wang, G. Wang, et al., All-optical synapse with directional coupler structure based on phase change material, *IEEE Photon. J.*, **13** (2021), 1–6. https://doi.org/10.1109/JPHOT.2021.3102132

99. O. Sharifipour, P. Keshavarzi, M. Danaie, All-optical plasmonic synapse based on phase change material suitable for neuromorphic circuits, *Opt. Quantum Electron.*, **57** (2025), 1–35. https://doi.org/10.1007/s11082-025-08261-6

100. P. Zhao, S. Yan, R. Xing, J. Yao, X. Ge, K. Li, et al., Homogeneous photoelectric reservoir computing system based on chalcogenide phase change materials, *Mater. Today Nano*, (2025), 100576. https://doi.org/10.1016/j.mtnano.2025.100576

101. L. Chua, Memristor-the missing circuit element, *IEEE Trans. Circuit Theory*, **18** (2003), 507–519.

102. G. N. Panin, O. O. Kapitanova, Memristive systems based on two-dimensional, in: *Advances in Memristor Neural Networks: Modeling and Applications*, 2018, pp. 67.

103. G. N. Panin, O. O. Kapitanova, Photomemristor structures based on 2D crystals for biocompatible information sensor systems, *Nanobiotechnology Rep.*, **16** (2021), 706–721. https://doi.org/10.1134/S2635167621060173

104. S. Song, J. Kim, S. M. Kwon, J. W. Jo, S. K. Park, Y. H. Kim, Recent progress of optoelectronic and all-optical neuromorphic devices: a comprehensive review of device structures, materials, and applications, *Adv. Intell. Syst.*, **3** (2021), 2000119. https://doi.org/10.1002/aisy.202000119

105. M. Zeng, Y. He, C. Zhang, Q. Wan, Neuromorphic devices for bionic sensing and perception, *Front. Neurosci.*, **15** (2021), 690950. https://doi.org/10.3389/fnins.2021.690950

106. J. Shen, Z. Cheng, P. Zhou, Optical and optoelectronic neuromorphic devices based on emerging memory technologies, *Nanotechnology*, **33** (2022), 372001. https://doi.org/10.1088/1361-6528/ac723f

107. J. Wang, Y. Zhu, L. Zhu, C. Chen, Q. Wan, Emerging memristive devices for brain-inspired computing and artificial perception, *Front. Nanotechnol.*, **4** (2022), 940825. https://doi.org/10.3389/fnano.2022.940825

108. S. Wang, L. Song, W. Chen, G. Wang, E. Hao, C. Li, et al., Memristor-based intelligent human-like neural computing, *Adv. Electron. Mater.*, **9** (2023), 2200877. https://doi.org/10.1002/aelm.202200877

109. X. Chen, Y. Xue, Y Sun, J. Shen, S. Song, M. Zhu, et al., Neuromorphic photonic memory devices using ultrafast, non-volatile phase-change materials, *Adv. Mater.*, **35** (2023), 2203909. https://doi.org/10.1002/adma.202203909

110. N. Youngblood, C. A. Rios Ocampo, W. H. Pernice, H. Bhaskaran, Integrated optical memristors, *Nat. Photonics*, **17** (2023), 561–572. https://doi.org/10.1038/s41566-023-01217-w

111. I. M. Kipelkin, S. A. Gerasimova, A. I. Belov, D. V. Guseinov, A. V. Kruglov, D. A. Serov, et al., Memristor-based model of neuronal excitability and synaptic potentiation, *Front. Neurosci.*, **18** (2024), 1456386. https://doi.org/10.3389/fnins.2024.1456386

112. M. N. Koryazhkina, A. V. Lebedeva, D. D. Pakhomova, I. N. Antonov, V. V. Razin, E. D. Budylina, et al., Investigation of in vitro neuronal activity processing using a CMOS-integrated ZrO_2 (Y)-based memristive crossbar, *Chaos Soliton. Fract.*, **191** (2025), 115959. https://doi.org/10.1016/j.chaos.2024.115959

113. S. N. Nikolaev, A. I. Iliasov, D. V. Ichetkin, A. V. Emelyanov, S. Y. Shabanov, A. V. Sitnikov, et al., Features of the resistive switching of memristors based on a $(CoFeB)_x(LiNbO_3)_{100-x}$ nanocomposite with a Ni electrode: Influence of temperature and magnetic field, *Nanobiotechnol. Rep.*, **20** (2025), 93–99. https://doi.org/10.1134/S263516762460250X

114. D. Martini, D. Angeli, G. Innocenti, A. Tesi, M. D. Marco, M. A. Forti, A Lyapunov function-based condition for nonoscillatory behaviors in a class of memristor circuits, *Int. J. Bifurc. Chaos*, **35** (2025), 2550151. https://doi.org/10.1142/S0218127425501512

115. D. Maldonado, C. Acal, H. Ortiz, A. M. Aguilera, J. E. Ruiz-Castro, A. Cantudo, et al., A comprehensive statistical study of the post-programming conductance drift in HfO_2-based memristive devices, *Mater. Sci. Semicond. Process.*, **196** (2025), 109668. https://doi.org/10.1016/j.mssp.2025.109668

116. A. Mehonic, D. Ielmini, K. Roy, O. Mutlu, S. Kvatinsky, T. Serrano-Gotarredona, et al., Roadmap to neuromorphic computing with emerging technologies, *APL Mater.*, **12** (2024), 100901. https://doi.org/10.1063/5.0179424

117. S. A. Gerasimova, A. V. Lebedeva, N. V. Gromov, A. E. Malkov, A. A. Fedulina, T. A. Levanova, et al., Memristive neural networks for predicting seizure activity, *Sovrem. Tehnol. Med.*, **15** (2023), 30–37. https://doi.org/10.17691/stm2023.15.4.03

118. S. V. Stasenko, A. N. Mikhaylov, V. B. Kazantsev, Control of network bursting in a model spiking network supplied with memristor-implemented plasticity, *Mathematics*, **11** (2023), 3888. https://doi.org/10.3390/math11183888

119. V. Van, *Optical Microring Resonators: Theory, Techniques, and Applications*, CRC Press, 2016.

120. Q. Zhang, H. Yu, M. Barbiero, B. Wang, M. Gu, Artificial neural networks enabled by nanophotonics, *Light Sci. Appl.*, **8** (2019), 42. https://doi.org/10.1038/s41377-019-0151-0

121. J. K. George, A. Mehrabian, R. Amin, J. Meng, T. F. De Lima, A. N. Tait, et al., Neuromorphic photonics with electro-absorption modulators, *Opt. Express*, **27** (2019), 5181–5191. https://doi.org/10.1364/OE.27.005181

122. M. Miscuglio, A. Mehrabian, Z. Hu, S. I. Azzam, J. George, A. V. Kildishev, et al., All-optical nonlinear activation function for photonic neural networks, *Opt. Mater. Express*, **8** (2018), 3851–3863. https://doi.org/10.1364/OME.8.003851

123. G. Mourgias-Alexandris, G. Dabos, N. Passalis, A. Totović, A. Tefas, N. Pleros, All-optical WDM recurrent neural networks with gating, *IEEE J. Sel. Top. Quantum Electron.*, **26** (2020), 1–7. https://doi.org/10.1109/JSTQE.2020.2995830

124. H. Zhang, J. Thompson, M. Gu, X. D. Jiang, H. Cai, P. Y. Liu, et al., Efficient on-chip training of optical neural networks using genetic algorithm, *ACS Photon.*, **8** (2021), 1662–1672. https://doi.org/10.1021/acsphotonics.1c00035

125. R. Hamerly, S. Bandyopadhyay, D. Englund, Asymptotically fault-tolerant programmable photonics, *Nat. Commun.*, **13** (2022), 6831. https://doi.org/10.1038/s41467-022-34308-3

126. B. Wu, S. Liu, J. Cheng, W. Dong, H. Zhou, J. Dong, et al., Real-valued optical matrix computing with simplified MZI mesh, *Intell. Comput.*, **2** (2023), 0047. https://doi.org/10.34133/icomputing.004

127. L. El Srouji, M. B. On, Y. J. Lee, M. Abdelghany, S. B. Yoo, Experimental demonstration of imperfection-agnostic local learning rules on photonic neural networks with Mach-Zehnder interferometric meshes, in: *Optical Fiber Communication Conference*, 2024. https://doi.org/10.1364/OFC.2024.M4C.1

128. M. B. On, Y. J. Lee, L. E. Srouji, M. Abdelghany, S. B. Yoo, Improving scalability of Mach-Zehnder interferometer based photonic computers via algorithm-hardware codesign, *J. Lightwave Technol.*, **42** (2024), 8014–8023. Available from: `https://opg.optica.org/jlt/abstract.cfm?URI=jlt-42-22-8014`

129. J. Faneca, T. D. Bucio, F. Y. Gardes, A. Baldycheva A., O-band N-rich silicon nitride MZI based on GST, *Appl. Phys. Lett.*, **116** (2020), 091105. https://doi.org/10.1063/1.5140350

130. B. Schrenk, Simplified coherent synaptic receptor for filterless optical neural networks, *IEEE J. Sel. Top. Quantum Electron.*, **28** (2022), 1–7. https://doi.org/10.1109/JSTQE.2021.3108573

131. M. V. Stephanie, F. Honz, N. Vokić, W. Boxleitner, M. Waltl, T. Grasser, et al., SOA-REAM assisted synaptic receptor for weighted-sum detection of multiple inputs, *J. Lightwave Technol.*, **41** (2022), 1258–1264. https://doi.org/10.1109/JLT.2022.3212111

132. C. Chen, S. J. Liu, M. L. Wang, S. G. Zhang, Y. L. Xiao, Phase-shift determination for a 4×4 intelligent photonic neural network with compatible learning, *Appl. Opt.*, **60** (2021), 2100–2108. https://doi.org/10.1364/AO.417935

133. G. Mourgias-Alexandris, N. Passalis, G. Dabos, A. Totović, A. Tefas, N. Pleros, A photonic recurrent neuron for time-series classification, *J. Lightwave Technol.*, **39** (2021), 1340–1347. Available from: `https://opg.optica.org/jlt/abstract.cfm?URI=jlt-39-5-1340`

134. S. Cheung, D. Liang, Y. Yuan, Y. Peng, Y. Hu, G. Kurczveil, et al., Ultra-power-efficient electrically programmable photonic memory on a heterogeneous III-V/Si optical computing platform, *arXiv*, preprint, arXiv:2303.12345, 2023. https://doi.org/10.21203/rs.3.rs-3098943/v1

135. Z. Wang, M. Xiang, F. Yang, K. Liu, J. Bao , D. Yang, et al., Ultrafast and high extinction ratio 1×4 electro-optical switch based on cascaded dual-output MZI, *IEEE Photon. J.*, **15** (2023), 1–8. https://doi.org/10.1109/JPHOT.2023.3266953

136. A. Cem, S. Yan, Y. Ding, D. Zibar, F. Da Ros, Data-driven modeling of Mach-Zehnder interferometer-based optical matrix multipliers, *J. Lightwave Technol.*, **41** (2023), 5425–5436. https://doi.org/10.1109/JLT.2023.3263235

137. M. V. Stephanie, L. Pham, A. Schindler, M. Waltl, T. Grasser, B. Schrenk, Neural network with optical frequency-coded ReLU, in: *Optical Fiber Communication Conference*, 2024. https://doi.org/10.1364/OFC.2024.M4C.2

138. C. Li, R. Pan, C. Gu, H. Guo, J. Li, Reconfigurable micro/nano-optical devices based on phase transitions: From materials, mechanisms to applications, *Adv. Sci.*, **11** (2024), 2306344. https://doi.org/10.1002/advs.202306344

139. R. Guirado, G. Perez-Palomino, M. Ferreras, E. Carrasco, M. Cano-Garcia, Dynamic modeling of liquid crystal-based metasurfaces and its application to reducing reconfigurability times, *IEEE Trans. Antennas Propag.*, **70** (2022), 11847–11857. https://doi.org/10.1109/TAP.2022.3209734

140. F. Ding, C. Meng, S. I. Bozhevolnyi, Electrically tunable optical metasurfaces, *Photon. Insights*, **3** (2024), R07. https://doi.org/10.3788/PI.2024.R07

141. C. Zhang, L. Cong, J. Zhang, H. Meng, S. Peng, S. Li, et al., Advanced metasurfaces: Precise modulations of light in space and time domains, *Adv. Photon.*, **8** (2026), 014003. https://doi.org/10.1117/1.AP.8.1.014003

142. I.-W. Chen, C. Y. Chan, P. Navarro, V. de Sars, E. Ronzitti, K. Oweiss, et al., High-throughput synaptic connectivity mapping using in vivo two-photon holographic optogenetics and compressive sensing, *Nat. Neurosci.*, **28** (2025), 2141–2153. https://doi.org/10.1038/s41593-025-02024-y

143. M. R. Eslami, Y. M. Banad, S. S. Sharif, Photonic crystal-based binary-to-gray converter: A low-power solution for optical neural network accelerators, in: *2025 IEEE Research and Applications of Photonics in Defense Conference (RAPID)*, 2025, pp. 1–2.

144. G. M. Lerman, J. P. Little, J. V. Gill, D. Rinberg, S. Shoham, Real-time in situ holographic optogenetics confocally unraveled sculpting microscopy, *Laser Photon. Rev.*, **13** (2019), 1900144. https://doi.org/10.1002/lpor.201900144

145. N. C. Pégard, A. R. Mardinly, I. A. Oldenburg, S. Sridharan, L. Waller, H. Adesnik, Three-dimensional scanless holographic optogenetics with temporal focusing, *Nat. Commun.*, **8** (2017), 1228. https://doi.org/10.1038/s41467-017-01031-3

146. M. H. Eybposh, V. R. Curtis, J. Rodríguez-Romaguera, N. C. Pégard, Advances in computer-generated holography for targeted neuronal modulation, *Neurophotonics*, **9** (2022), 041409. https://doi.org/10.1117/1.NPh.9.4.041409

147. Z. Ge, C. Wang, J. Huang, E. Y. Lam, Event-driven neuromorphic holography for dynamic particle imaging, *Opt. Lett.*, **50** (2025), 1496–1499. https://doi.org/10.1364/OL.548088

148. V. R. Daria, Holographic photonic neuron, *Neuromorph. Comput. Eng.*, **1** (2021), 024009. https://doi.org/10.1088/2634-4386/ac3ba5

149. F. T. Arecchi, Feature binding as neuron synchronization: quantum aspects, *Braz. J. Phys.*, **35** (2005), 411–417. https://doi.org/10.1590/S0103-97332005000200008

150. R. Meucci, F. Salvadori, M. V. Ivanchenko, K. Al Naimee, C. Zhou, F. T. Arecchi, S. Boccaletti, J. Kurths, Synchronization of spontaneous bursting in a CO_2 laser, *Phys. Rev. E*, **74** (2006), 066207. https://doi.org/10.1103/PhysRevE.74.066207

151. M. Naruse, Y. Terashima, A. Uchida, S. J. Kim, Ultrafast photonic reinforcement learning based on laser chaos, *Sci. Rep.*, **7** (2017), 8772. https://doi.org/10.1038/s41598-017-08585-8

152. B. Kelleher, B. Tykalewicz, D. Goulding, N. Fedorov, I. Dubinkin, T. Erneux, et al., Two-color bursting oscillations, *Sci. Rep.*, **7** (2017), 8414. https://doi.org/10.1038/s41598-017-08751-y

153. R. Lang, K. Kobayashi, External optical feedback effects on semiconductor injection laser properties, *IEEE J. Quantum Electron.*, **16** (1980), 347–355. https://doi.org/10.1109/JQE.1980.107047

154. B. Kelleher, C. Bonatto, G. Huyet, S. P. Hegarty, Excitability in optically injected semiconductor lasers: Contrasting quantum-well- and quantum-dot-based devices, *Phys. Rev. E*, **83** (2011), 026207. https://doi.org/10.1103/PhysRevE.83.026207

155. J. Tiana-Alsina, C. Quintero-Quiroz, M. Panozzo, M. C. Torrent, C. Masoller, Experimental study of modulation waveforms for entraining the spikes emitted by a semiconductor laser with optical feedback, *Sci. Rep.*, **8** (2018), 10909. https://doi.org/10.1364/OE.26.009298

156. M. M. Jaber, A. A. Hemed, The chaotic behavior of an optical artificial neuron, *Fiber Integr. Opt.*, **43** (2024), 235–260. https://doi.org/10.1080/01468030.2024.2411450

157. Y. Nie, B. Yang, D. Wang, T. Wang, J. Wang, Z. Wang, et al., Integrated laser graded neuron enabling high-speed reservoir computing without feedback loop, *Optica*, **11** (2024), 1690–1699. https://doi.org/10.1364/OPTICA.537231

158. P. R. Prucnal, B. J. Shastri, T. Ferreira de Lima, M. A. Nahmias, A. N. Tait, Recent progress in semiconductor excitable lasers for photonic spike processing, *Adv. Opt. Photon.*, **8** (2016), 228–299. https://doi.org/10.1364/AOP.8.000228

159. V. N. Chizhevsky, V. A. Kulchitsky, S. Y. Kilin, Artificial spiking neuron based on a single-photon avalanche diode and a microcavity laser, *Appl. Phys. Lett.*, **119** (2021), 041101. https://doi.org/10.1063/5.0055392

160. N. V. Lakhmitskii, V. N. Chizhevsky, S. Y. Kilin, Stochastic resonance in optoelectronic artificial spiking neuron, *J. Appl. Spectrosc.*, **90** (2023), 1069–1073. https://doi.org/10.1007/s10812-023-01634-3

161. V. N. Chizhevsky, N. V. Lakhmitskii, Improvement of signal propagation in the optoelectronic artificial spiking neuron by vibrational resonance, *Phys. Rev. E*, **109** (2024), 014211. https://doi.org/10.1103/PhysRevE.109.014211

162. A. Banerjee, J. D. Hart, R. Roy, E. Ott, Machine learning link inference of noisy delay-coupled networks with optoelectronic experimental tests, *Phys. Rev. X*, **11** (2021), 031014. https://doi.org/10.1103/PhysRevX.11.031014

163. A. Skalli, S. Sunada, M. Goldmann, M. Gebski, S. Reitzenstein, J. A. Lott, et al., Model-free front-to-end training of a large high performance laser neural network, *arXiv*, preprint, arXiv:2503.16943, 2025.

164. S. Gu, K. Li, P. Zhou, N. Li, Parallel optical chaos generation and ultrafast photonic decision-making based on a single quantum dot spin-VCSEL, *Chaos Soliton. Fract.*, **191** (2025), 115874. https://doi.org/10.1016/j.chaos.2024.115874

165. N. Li, Y. Feng, Y. Zhang, Y. Huang, P. Zhou, A reconfigurable photonic signal processor based on spiking VCSEL neurons, *J. Lightwave Technol.*, (2025), 6732 – 6743. https://doi.org/10.1109/JLT.2025.3559894

166. D. Owen-Newns, L. Jaurigue, J. Robertson, A. Adair, J. A. Jaurigue, K. Lüdge, Photonic spiking neural network built with a single VCSEL for high-speed time series prediction, *Commun. Phys.*, **8** (2025), 110. https://doi.org/10.1038/s42005-025-02000-9

167. P. Zhao, R. Ji, J. Lao, W. Xu, C. Jiang, C. Luo, et al., Two-terminal organic optoelectronic synapse based on poly (3-hexylthiophene) for neuromorphic computing, *Org. Electron.*, **100** (2022), 106390. https://doi.org/10.1016/j.orgel.2021.106390

168. L. Jiang, X. Wu, F. Ni, X. Wang, L. Qiu, Vertical phase separation to regulate the structural morphology of organic semiconductors and its applications, *ACS Mater. Lett.*, **8** (2026), 1–15. https://doi.org/10.1021/acsmaterialslett.5c01278

AIMS Press

©2026 the Author(s), licensee AIMS Press. This is an open access article distributed under the terms of the Creative Commons Attribution License (https://creativecommons.org/licenses/by/4.0)